Journal of Volcanology and Geothermal Research 468 (2025) 108436

Contents lists available at ScienceDirect

Journal of Volcanology and Geothermal Research

journal homepage: www.journals.elsevier.com/journal-of-volcanology-and-geothermal-research

Revealing the timing and dispersal of large explosive eruptions at Aso volcano (Japan) by integrating proximal and distal tephra records over the last 130 kyrs

Sophie O. Vineberg [a,*], Paul G. Albert [b,*], Danielle McLean [a], Takehiko Suzuki [c], Yasuo Miyabuchi [d], Hideo Hoshizumi [e], Hannah M. Buckland [b], Gwydion Jones [b], Fumikatsu Nishizawa [f], Richard A. Staff [a,g], Keitaro Yamada [h], Ikuko Kitaba [h,i], Junko Kitagawa [j], Christina J. Manning [k], SG14 Project Members[1], Takeshi Nakagawa [h], Victoria C. Smith [a]

[a] Research Laboratory for Archaeology and the History of Art, School of Archaeology, University of Oxford, Oxford OX1 3TG, UK
[b] Department of Geography, Swansea University, Swansea SA2 8PP, UK
[c] Department of Geography, Tokyo Metropolitan University, Tokyo 192-0397, Japan
[d] Centre for Water Cycle, Marine Environment and Disaster Management, Kumamoto University, Kumamoto 860-8555, Japan
[e] Geological Survey of Japan, AIST, Tsukuba, Ibaraki 305-8567, Japan
[f] Kanagawa Prefectural Museum of Natural History, Odawara 250-0031, Japan
[g] Department of Scientific Research, The British Museum, London WC1B 3DG, UK
[h] Research Centre for Paleoclimatology, Ritsumeikan University, Kusatsu, Shiga 525-8577, Japan
[i] Fukui Prefectural Satoyama-Satoumi Research Institute, Wakasa 919-1331, Japan
[j] Varve Museum, Wakasa, Fukui 919-1331, Japan
[k] Department of Earth Sciences, Royal Holloway, University of London, Egham, Surrey TW20 0EX, UK

ARTICLE INFO

Keywords:
Aso
Aso-4
Tephra
Volcanic glass geochemistry
Cryptotephra
Lake Suigetsu
Eruption history

ABSTRACT

Aso caldera in central Kyushu, SW Japan, is one of the largest and most active volcanoes in the world. The Aso system has experienced four caldera-forming eruptions (Aso-1 to -4) and inter-caldera activity from multiple central cones. This study provides detailed glass geochemistry of previously uncharacterised near-source, predominantly silicic, tephra units so that they can be correlated to ashfall layers preserved in distally located sedimentary records. Here the near-source glass data from twenty eruption deposits are integrated with the distal tephra fall deposits recorded in the high-resolution Lake Suigetsu record (situated approximately 525 km to the north-east), to better constrain the eruption timing, frequency, and ash dispersal of pre-30 ka Aso eruptions. The glass chemistry of these large Aso eruptions typically straddles the trachy-dacitic to rhyolitic compositional boundary. While some units share overlapping or similar glass chemistries, many can be distinguished from each other using major (SiO_2, K_2O, CaO and FeO_t) and trace element (Sr) contents. The newly available near-source volcanic glass dataset has enabled the identification and correlation of an additional six tephra and cryptotephra deposits within the Lake Suigetsu record to known Aso eruptions. Consequently, nine of the twenty deposits in the Lake Suigetsu record (SG06/SG14 cores) displaying an Aso glass composition have now been correlated to near-source eruption units; these include, from youngest to oldest: Aso-Kpfa, Upper ACP4, Lower ACP4, ACP6, YmP5, Aso-4, Aso-ABCD, Aso-EF and Aso-HI. Significantly, the identification of these tephra deposits in Lake Suigetsu provides improved age estimates for the eruptions, and helps constrain the repose periods between eruptions; for instance ~400 years are resolved between two eruptions associated with the ACP4 Plinian activities. Our integrated proximal-distal record also indicates a higher frequency of activity in the 10 kyrs leading up to Aso-4 caldera-forming eruption. Eleven Aso-derived eruption deposits in the Lake Suigetsu record have not yet been recognised in the exposed near-vent sequences, perhaps suggesting that Aso caldera has been responsible for more silicic high-intensity eruptions and widespread ashfall events than previously thought. This research demonstrates the merit of integrating proximal-distal records to better constrain eruption timing, frequencies and ash dispersals of pre-historic events.

* Corresponding authors.
E-mail address: p.g.albert@swansea.ac.uk (P.G. Albert).
[1] www.suigetsu.org

https://doi.org/10.1016/j.jvolgeores.2025.108436
Received 23 February 2025; Received in revised form 8 July 2025; Accepted 1 September 2025
Available online 6 September 2025

1. Introduction

Large caldera-forming eruptions (i.e. those with a volcanic explosivity index [VEI] or Magnitude [M] ≥6; Pyle, 2000; Newhall and Self, 1982) have significant impacts associated with voluminous ignimbrites, landscape modification from the caldera collapse, and widespread ashfall. Tephra deposits ejected during such large explosive eruptions can be incredibly widespread, being dispersed 1000s km from vent and forming key chrono-stratigraphic markers in the sediments in which they are deposited. Once identified and geochemically characterised, these aid in the synchronisation and dating of sedimentary sequences across large geographical areas (e.g. Davies et al., 2024; McLean et al., 2016, 2018; Sun et al., 2014; Lane et al., 2013; Wulf et al., 2012).

Accurately reconstructing the eruption histories of highly productive volcanoes is essential to determining the number, frequency and scale of widespread ashfall events, contributing a key component of hazard assessments. Whilst near-source (proximal) eruption sequences are fundamental to the reconstruction of past volcanic histories by providing stratigraphic, chronological and geochemical constraints, these deposits can be destroyed and/or buried by the eruption deposits of more recent activities, including caldera-forming events. This means that accessible proximal stratigraphies alone cannot always provide a complete eruption record for very active volcanoes. Palaeosols are typically used to demarcate different eruption units, however they can take hundreds of years to develop, thus closely spaced eruptions, occurring on shorter timescales can be erroneously grouped into a single eruption deposit, particularly in the absence of any additional evidence of quiescence (e.g., erosional unconformities). Furthermore, palaeosols are often absent due to erosional processes at the volcano, and this grouping of eruption deposits results in near-source eruption underreporting (e.g. Kiyosugi et al., 2015). Potential for eruption underreporting is particularly relevant to the highly active caldera volcanoes of Japan, these are source of some of the largest known caldera-forming events of the past 200 kyrs, blanketing Japan and the surrounding seas in ashfall (e.g. Machida and Arai, 2003; Smith et al., 2013; Ikehara, 2015; Mahony et al., 2016; Schindlbeck et al., 2018; Albert et al., 2019a; McLean et al., 2020; Matsu'ura et al., 2021).

Fortunately, distal sedimentary archives (e.g. lacustrine and marine cores) can help overcome near-source preservation and accessibility issues, not only do they preserve tephra deposits associated with the largest eruptions, they also often provide a record of small- and medium-sized eruptions, if they are relatively close to the source volcano (e.g. Wulf et al., 2004; Bourne et al., 2010; Wutke et al., 2015; McLean et al., 2020). Only once the tephra deposits have been correlated to a particular volcano and eruption using the glass geochemistry, can the distal records be used to gain greater insights into timing, frequency and repose periods (e.g. Campi Flegrei [Italy]; Sulpizio et al., 2014; Vineberg et al., 2023; Albert et al., 2019b; Fernandez et al., 2024). The integration of the near-source and distal tephra records are therefore key to developing accurate tephrochronological frameworks for individual volcanic systems, and thus elucidating comprehensive eruption records.

In Japan, the correlation of near-source eruption deposits to tephra layers preserved in the Lake Suigetsu sedimentary archive (Fig. 1C) has enabled the high precision chronology of the site (e.g., Bronk Ramsey et al., 2012, 2020; Schlolaut et al., 2012, 2018) to provide very precise constraints upon the timing of past eruptions and the relative timing of different eruptions, establishing Lake Suigetsu as key tephro-stratotype for east Asia (e.g., Smith et al., 2013; McLean et al., 2016, 2018, 2020; Albert et al., 2018, 2019a, 2024; Vineberg et al.,2024). Distal eruption deposits associated with caldera-forming eruptions at Japanese volcanoes (Fig. 1A), and from those even further afield (e.g., North Korea/China), have been identified throughout the Lake Suigetsu sediments spanning the last ~150 kyrs, either as visible or non-visible tephra (cryptotephra) deposits (e.g., B-Tm, K-Ah, AT, Aso-4; K-Tz; Ata, Toya; Vineberg et al., 2024; Albert et al., 2019a; McLean et al., 2016, 2018; Smith et al., 2013). The preservation and identification of cryptotephra deposits throughout the Lake Suigetsu sedimentary sequence has revealed numerous eruptions from these caldera systems, most notably frequent ashfall events from Aso volcano, many of which have not yet been assigned to deposits in the near-source setting (see: Vineberg et al., 2024; McLean et al., 2020).

The Aso volcano is part of the Central Volcanic Region (CVR) and located on Kyushu Island in the southwestern Japan Arc (Fig. 1A). It is one of the most hazardous volcanic systems on Earth, and also one of the most active volcanic complexes in Japan. Since ~270 ka Aso has experienced four gigantic caldera-forming eruptions (M 7 and 8. Aso-1 (266 ± 14 ka) and Aso-2 (141 ± 5.0 ka) have estimated bulk volumes exceeding 50 km^3 (Ono et al., 1977; Kaneko et al., 2015). The penultimate caldera-forming eruption, Aso-3 has age estimates of between 115 and 130 ka (Kaneko et al., 2015), and a bulk volume estimate of more than 180 km^3 (Hoshizumi et al., 2024). The Aso caldera (18 × 25 km) is the product of the last caldera-forming eruption, Aso-4, which is dated to 86.4 ± 1.1 ka (2σ; $^{40}Ar/^{39}Ar$;Albert et al., 2019a), an age consistent with its distal ashfall deposits occurring within sediments attributed to Marine Isotope Stage (MIS) 5b (Aoki, 2008). Integrating near-source thickness mapping of the Aso-4 pyroclastic density current (PDC) deposits (Hoshizumi et al., 2023) and distal tephra fall has led to Aso-4 total eruptive volume estimates exceeding 900 km^3, significantly greater than previous estimates (~600 km^3), and suggesting this event was ≥M8.0 (Takarada and Hoshizumi, 2020). Indeed, Aso-4 provides a key widespread tephrostratigraphic marker that is found interbedded within the eruption stratigraphies of other volcanic systems (marked/shown on Fig. 1D; e.g. Albert et al., 2019a; Matsu'ura et al., 2014; Machida and Arai, 2003; Nagaoka et al., 2001) and is frequently identified in marine and terrestrial sedimentary records across East Asia (e.g. Matsu'ura and Komatsubara, 2024; Derkachev et al., 2019; Sagawa et al., 2018; Lim et al., 2013; Smith et al., 2013; Nagahashi et al., 2004a, 2004b).

Near-vent eruptive stratigraphies associated with airfall tephra deposits from Aso are to date predominantly preserved and identified to the ENE, E and SE of the caldera wall, interbedded between the PDC deposits associated with caldera-forming events (e.g. Miyabuchi et al., 2003; Miyabuchi, 2009; Hoshizumi et al., 2022). Detailed tephrostratigraphic frameworks have been developed for the eruption units spanning approximately the last 130 kyr using these proximal outcrops (e.g., Hoshizumi et al., 2022; Miyabuchi, 2009, 2011; Ono and Watanabe, 1983; Ono et al., 1977). However, the lack of detailed (volcanic glass) geochemical characterisation of these units to date has prevented them from being reliably correlated across greater geographical areas. For instance, twenty volcanic deposits (four visible tephra and sixteen cryptotephra layers) identified within the Lake Suigetsu sediments spanning 120–30 ka have been geochemically correlated to Aso volcano (Vineberg et al., 2024; McLean et al., 2020; Albert et al., 2019a; Smith et al., 2013). Only four of these deposits have been correlated to their proximal counterpart and a specific eruption unit. These proximal-distal correlations between Lake Suigetsu and Aso have constrained the ages of the following eruption deposits: Aso-Kpfa (SG14–2752; 32,512 ± 271 cal. BP [2σ]; McLean et al., 2020), Aso central cone pumice (ACP) 4 (SG06–3912; 50.0 ± 0.3 ka cal. BP [2σ]; Albert et al., 2019a) and Aso-ABCD (SG06–5287; 97.9 ± 6.0 ka [2σ]; Albert et al., 2019a; Smith et al., 2013). Finally, the correlation of the visible tephra SG06–4963 to the Aso-4 deposits allows the near-source $^{40}Ar/^{39}Ar$ age determination of the eruption (86.4 ± 1.1 ka [2σ]) to be imported into the age-depth model of Lake Suigetsu, helping to constrain the chronology of the deeper sections of the core (Albert et al., 2019a).

This study provides detailed geochemical characterisation of the matrix glass of numerous previously uncharacterised, near-source Aso eruptive units, with the aim to use these data to facilitate the integration of proximal and distal eruption records. In particular, this study intends to link Aso tephra deposits to those preserved within arguably the most comprehensive and high-resolution distal ash fall record in Japan to date, Lake Suigetsu. The ultimate aim being to better constrain the

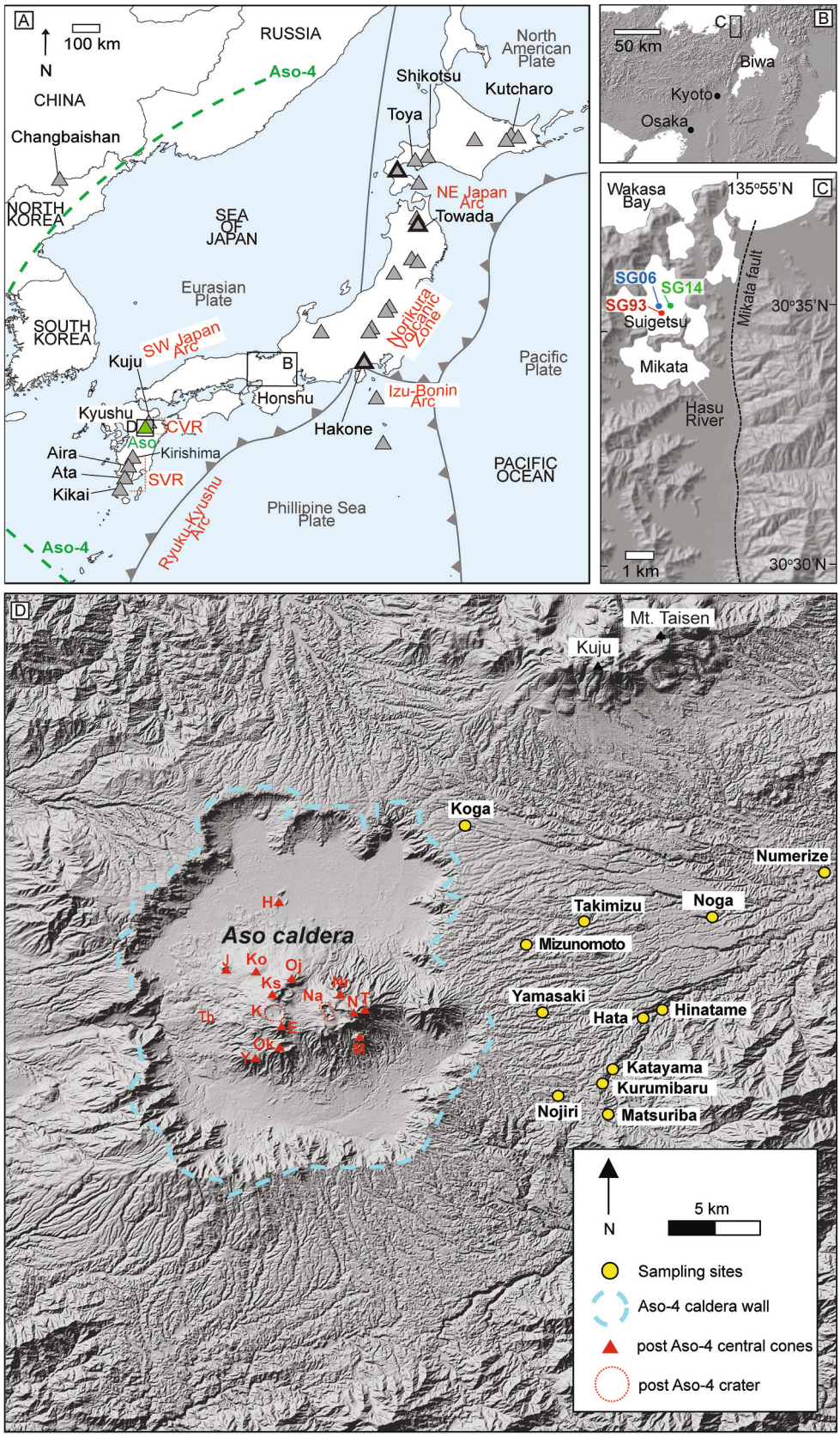

(caption on next page)

Fig. 1. **(A)** Volcanoes (triangles) that have been active in and around Japan in the Late Quaternary. The Aso caldera and focus of this study is shown by a green triangle. The green dashed line denotes the ash dispersal boundary for the Aso-4 caldera-forming eruption following Machida (2002). The red labels are the different volcanic arcs: SVR = Southern Volcanic Region; CVR = Central Volcanic Region; SWJA = South West Japan Arc; NEJA = North East Japan Arc. **(B)** Proximity of the distal study site Lake Suigetsu (located within the C square) to Lake Biwa and major Japanese cities. **(C)** Location of Lake Suigetsu which is part of the five Mikata Lake system, adjacent to the Wakasa Bay. The positions of all three coring campaigns are marked (b and c modified after Nakagawa et al., 2005). **(D)** Locations of near-source (proximal) stratigraphic sections discussed in this study (yellow circles). The blue dashed line denotes the Aso-4 caldera walls. The red triangles/labels mark peaks of the post Aso-4 central cones of Aso volcano: E: Eboshidake, H: Honzuka, J: Janoo, Ko: Komezuka, Ks: Kishimadake, M: Maruyama, N: Nakadake, Nr: Naraodake, Oj: Ojodake, Ok: Okamadoyama, T: Takadake, Tb: Takanoobane lava, Y: Yomineyama. The red dashed lines denote caldera walls from post Aso-4 central cone eruptions: K: Kusasenrigahama crater, Na: Nakadake crater. (For interpretation of the references to colour in this figure legend, the reader is referred to the web version of this article.)

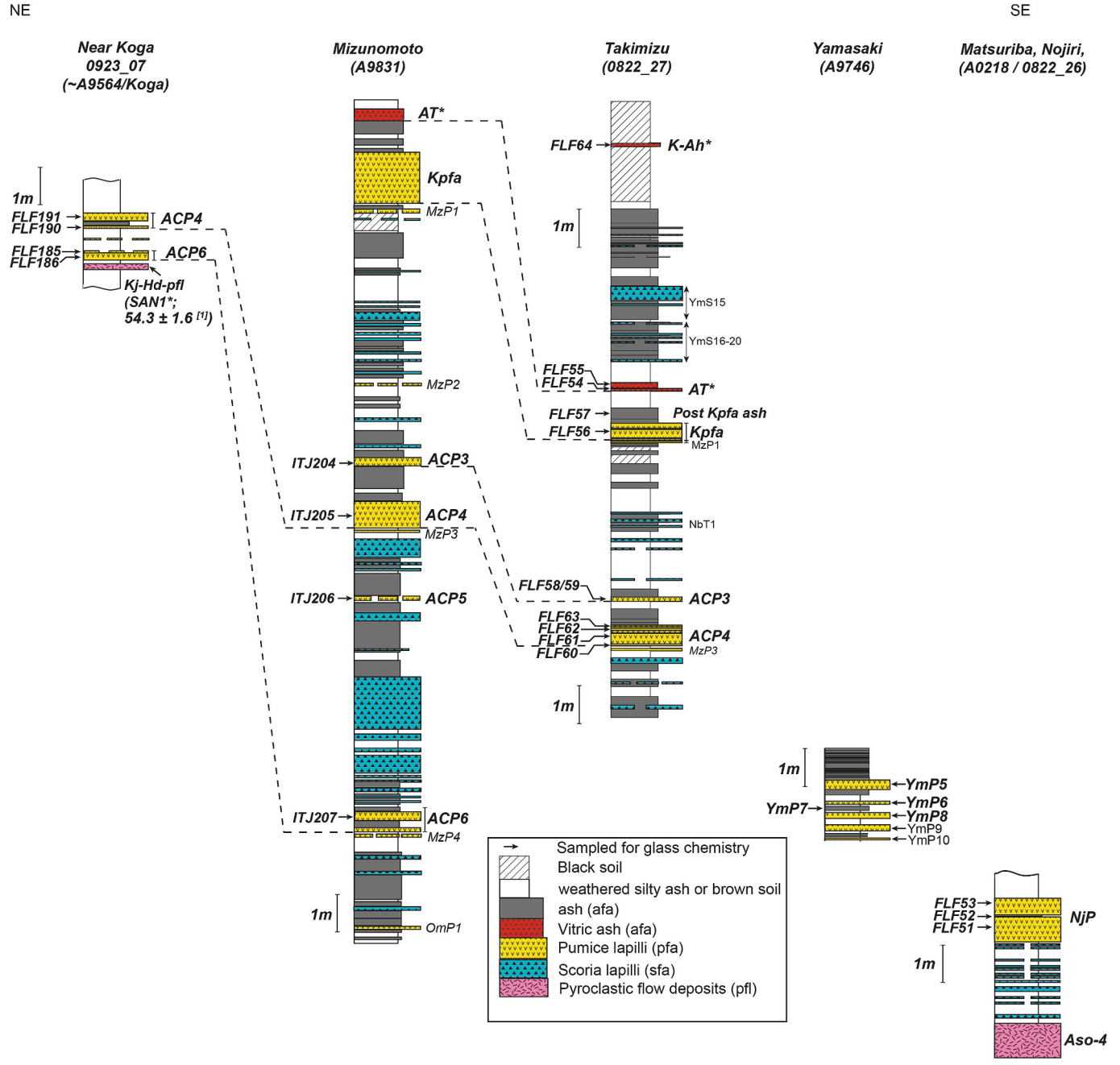

Fig. 2. Sampled sections containing tephra deposits erupted since the Aso-4 caldera-forming eruption, these sections follow those reported in Miyabuchi (2009), where the entire sequences are described. Those units in bold italics have been sampled for chemical analysis. ITJ prefix sample numbers at Mizunomoto relate to those units previously characterised in Albert et al. (2019a). Tephra deposits relating to external volcanic sources and widespread tephra deposits are marked by *, and these include the Aira-Tanzawa (AT), and the Kuju-Handa pyroclastic flow (Kj-Hd-fl), the latter is correlated to the SAN1 marine layer and Lake Suigetsu tephra SG06–4141 dated at 54.3 ± 1.6 ka (Albert et al., 2019a). The composite of post-Aso-4 tephrostratigraphy as reported in Miyabuchi (2009) can be found as **SFig. 1**.

eruption timings, frequencies, and ash dispersals of past Aso eruptions. This integrated proximal-distal tephrostratigraphic framework will facilitate the identification of Aso tephra deposits in other distal sedimentary archives in and around Japan, thus providing improved constraints being placed on the scale of past eruptions at Aso volcano. Here we focus on the chemical characterisation of more felsic fall deposits found beyond the caldera-wall, predominantly pumice lapilli and ash fall units that are most widely traced between geological exposures (e.g. Miyabuchi et al., 2003; Miyabuchi, 2009; Hoshizumi et al., 2022). Fall deposits thicknesses range from those that are >1 m thick at sites ~13 km E of the caldera-wall, to thinner units which are ≥10 cm thick at distances of 3 to 4 km. Units targeted for chemical analysis are interpreted as being associated with the largest explosive eruptions at Aso since the penultimate caldera-forming eruption at the volcano (Aso-3). These eruptions are considered most likely to have generated widespread ash dispersals, and potentially deposited ash fall on Lake Suigetsu >525 km away (Fig. 1A), along with other sedimentary archives in and around Japan. Here we focus on eruptions in the timeframe extending from 30 to 130 ka, as there are numerous Aso derived tephra layers preserved within the high-resolution Lake Suigetsu record spanning this time interval (Smith et al., 2013; Albert et al., 2019a; McLean et al., 2020; Vineberg et al., 2024).

2. Aso eruption history spanning 130–30 ka based on proximal exposures

Here we outline the physical and known geochemical features of many of the major silicic tephra deposits erupted from Aso volcano between the Aso-3 caldera-forming event (~130 ka; see below) and the AT tephra (a widespread marker tephra associated with the last caldera-forming eruption at Aira volcano, 200 km south of Aso; dated to ~30 ka; Smith et al., 2013). Owing to the prevailing westerlies, these deposits are best preserved in near-source outcrops located to the east, but also the south-east and north-east of the Aso-4 caldera wall (Fig. 1D; Fig. 2–3). These exposures or those in close proximity have previously been stratigraphically logged by Miyabuchi et al. (2003), Miyabuchi (2009), and Hoshizumi et al. (2022). Here we sampled the major pumiceous (silicic) eruption units from these stratigraphies for new major and trace element volcanic glass geochemical analyses. Scoria deposits were also sampled but were frequently too poorly preserved to enable reliable glass analysis. Details of the main eruption units sampled, including their eruption volumes (reported throughout as tephra volumes), magnitude (calculated using the tephra volume as in Pyle (2000), assuming a magma density of 2300 kg/m^3 and tephra density of 1000 kg/m^3), and dominant dispersal direction based on extensive field mapping (e.g., Hoshizumi et al., 2022; Miyabuchi, 2009), are summarised in Table 1, along with their age estimates.

2.1. Post-Aso-4 (<86 ka)

Post-caldera cones have developed near the centre of the caldera since the Aso-4 eruption (<86 ka; Ono and Watanabe, 1985). The total thickness of these post-Aso-4 tephra deposits is ~100 m on the eastern caldera rim (Watanabe and Fujimoto, 1992). Stratigraphically between the Aso-4 ignimbrite and the AT tephra, Miyabuchi (2009) reports more than twenty major silicic pumice bearing tephra beds, traceable between near-source sequences beyond the caldera-wall.

There are several minor scoria-fall deposits interspaced by weathered ash and soil between the Aso-4 and the Nojiri pumice (NjP) (Matsuriba/Nojiri; Fig. 2). However, many of these deposits are more mafic in composition and have become heavily weathered (Miyabuchi, 2011). The NjP is the first thick tephra deposit identified beyond the Aso caldera-walls and above the Aso-4 eruption deposit. It consists of extremely weathered pale-yellow pumice clasts, and is divided into lower and upper parts by an olive-brown 10 cm thick silty ash (Miyabuchi, 2009). It is considered one of the largest eruption events (likely M 4 to 5) to have occurred from the post-Aso central pumice cones. It is found in outcrops SE and is ~1.3 m thick at Matsuriba, 6 km beyond the caldera rim (Fig. 1D). NjP is absent at outcrops to the NE (Miyabuchi, 2009) suggesting that the dispersal may be confined to the southeast.

Directly above the NjP tephra, there is a ~ 4.5 m thick sequence of alternating pumice and scoria layers, interbedded with palaeosols (at the site of Matsuriba; Fig. 2). Stratigraphically, above this, at the site of Yamasaki, a series of alternating stratified pumice, scoria and ash fall deposits, collectively referred to as the Yamasaki Pumice (YmP) Series are recognised (Miyabuchi et al., 2003; Miyabuchi, 2009). Spanning more than 15 m in certain localities (SFig. 1), these deposits comprise of primary tephra units, weathered ash layers and palaeosols (Fig. S1). This sequence of deposits has been divided into thirteen different eruption deposits, which are labeled the YmP13 to 1, the oldest being 13 and youngest 1, with the eruptions responsible thought to span ca. 77–61 ka (Miyabuchi et al., 2003). Given some of these deposits are separated by thin soil beds, it suggests repose intervals with little or no eruptive activity, while the deposit thicknesses are greater to the east of the caldera, indicating a dominant ESE to ENE dispersal (Miyabuchi et al., 2003). The upper ~8 m includes five units of thick well-stratified ash layers and pumice beds (YmP5 to 1) separated by soils (Fig. S1; Miyabuchi, 2009). The YmP5 fall deposits is the thickest (up to 2.5 m), with the lower section comprised of alternating ash and pumice beds, whereas the middle and upper sections of the YmP5 tephra deposit are characterised by scoria fall deposits with thin ash layers (Fig. S1; Miyabuchi, 2009). The pumice fall deposit of YmP5 is identified as the key marker of the YmP Series (Miyabuchi et al., 2003; Miyabuchi, 2009) due to the thickness of the pumice beds at multiple localities, making it the most prominent and easily recognisable unit within the YmP Series.

Stratigraphically above the Yamasaki Pumice series and below the AT (~30 ka) marker are four pumice fall units known as the Aso central cone pumice (ACP) deposits, which are named sequentially from oldest to youngest ACP6, ACP5, ACP4, ACP3, and are routinely identified in outcrops east and northeast of the caldera wall (see: Miyabuchi, 2009, 2011). These deposits vary in thickness between localities, and are separated by palaeosols and scoria units, with the former indicating periods of time elapsed between each of these eruptions (Fig. 2; SFig. 1; Miyabuchi, 2009).

To the NE at Koga (A9564; Miyabuchi, 2009) the lowermost of these units, the ACP6 fall deposit, is preserved directly above a distal tephra from Kuju volcano (NE of the caldera; Fig. 1D). This deposit is associated with Kuju-Handa (Kj-Hd) Ignimbrite, which is preserved distally as ash fall at Lake Suigetsu (SG06–4141), where it is dated at 54.4 ± 1.6 ka (Fig. 2; Albert et al., 2019a, 2019b; Smith et al., 2013). The ACP6 can be traced between near-source outcrops and has a bulk volume of 0.21 km^3 (Takada, 1989). It is comprised of alternating beds, divided into seven units; Units 1, 3 and 6 are clast supported pumice lapilli deposits, whereas units 2, 4, 5 and 7 are massive or stratified ash deposits. The number of fall units present varies between localities, along with the degree of sorting (Miyabuchi et al., 2003; Miyabuchi, 2009, 2011). The overlaying ACP5 is a smaller volume pumice-fall deposit, with a bulk volume of 0.15 km^3 (Miyabuchi, 2009, 2011). Two further silicic eruptions occurred from vents in the western part of Aso caldera between ~54 and ~51 ka, ACP4 and ACP3 (Table 1). The ACP4 is considered the largest of the four pumice cone eruptions, with bulk volume of 0.43 km^3, while the ACP3 is the smallest with a bulk volume of 0.07 km^3 (Miyabuchi, 2009). The ACP4 is divided into four sub-units that are comprised of yellow pumice lapilli and ash fall beds (see Miyabuchi, 2011). The ACP4 has been correlated to the visible SG06–3912 tephra preserved in Lake Suigetsu (Albert et al., 2019a), with a recently updated age of 48.7 ± 0.19 ka that is based on the age-depth model of the site (Vineberg et al., 2024). The overlying ACP3 is preserved above a palaoesol, and this Plinian pumice fall deposit is chrono-stratigraphically associated with the rhyolitic Takanoobane lava flow which has been K/Ar dated to 51.0 ± 5.0 ka (Matsumoto et al.,

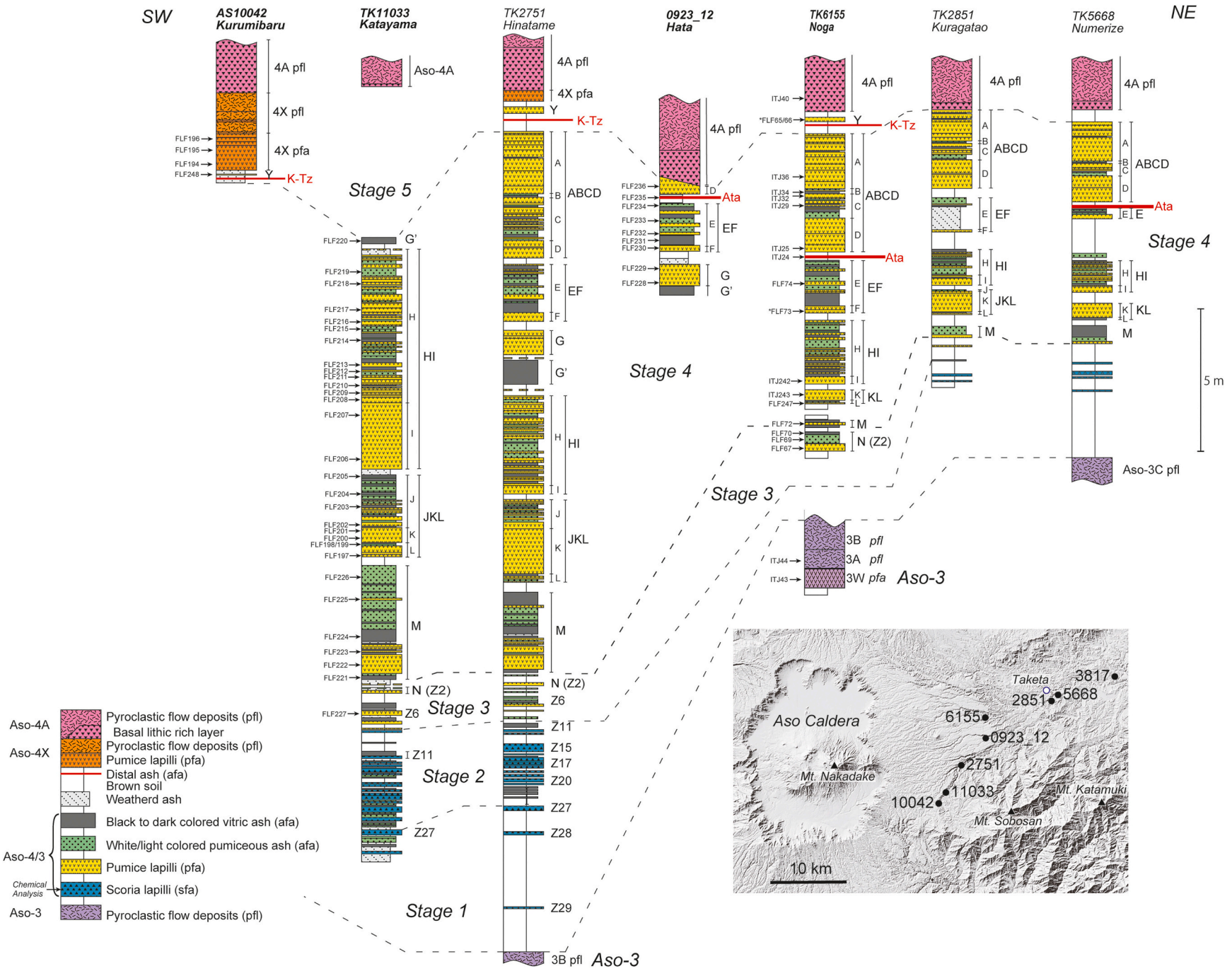

Fig. 3. Stratigraphic relationships of the Aso units preserved between Aso-3 (~130 ka) and Aso-4 (~86 ka) eruptions at sites located to the east of the caldera walls. The stratigraphic logs have been modified from Hoshizumi et al. (2022). The inset map shows the position of the sampling sites targeted here. Sampling positions are marked by arrows, those sample numbered with a ITJ prefix related to sample analysed in Albert et al. (2019a) from the Noga sequence.

Table 1
Key explosive eruptions defined from near-source (proximal) exposures located around Aso volcano stratigraphically positioned between the tephra deposits of the Aso-3 (~130 ka) and AT (Aira; ~30 ka) caldera-forming events. Dispersal and tephra volumes follow Hoshizumi et al., 2022 and Miyabuchi (2009). Eruption age references are as follows: a: McLean et al. (2020); b: Albert et al. (2019a); c: Miyabuchi (2009); d: Hoshizumi et al. (2022). * indicates an $^{40}Ar/^{39}Ar$ age. ^ Stage 3 includes Aso-N, which is equivalent to Z2 (Hoshizumi et al. (2022), and referred to as Aso-N (Z2) in this contribution. Note that the Yamasaki Pumices (YmP) 1 to 13 represents a series of pumice fall units interbedded within well-stratified ash and scoria beds, and separated in some instances by thin palaeosols, thus these deposits represent a series of eruptive events, as outlined in Miyabuchi (2009).

Stage of activity	Eruptions	Tephra	Previous correlative in Lake Suigetsu	Magnitude (M)	Tephra Volume (km^3)	Dispersal	Age (ka) (2σ)
Post-caldera	Aso-Kpfa	Aso-Kpfa	SG14–2752	5.3	2.21	E and S	32.5 ± 0.3[a]
	ACP3	ACP3	–	3.8	0.07	ENE	>51[b]
	ACP4	ACP4	SG06–3912	4.6	0.43	NE	50.0 ± 0.3[b]
	ACP5	ACP5	–	4.2	0.15	NE	>ACP4; <ACP6
	ACP6	ACP6	–	4.3	0.21	NE	~60[c]
	YmP-1 to 13	YmP-1 to 13	–	–	–	ESE - ENE	>ACP6; <NjP
	NjP	NjP	–	–	–	SE	~84[c]
Aso-4	Aso-4	Aso-4	SG06–4963	≥8.0	>600	–	86.4 ± 1.1[b]*
	Aso-4X	Aso-4X	–	–	–	–	>Aso-4; <Aso-Y
Stage 5	Aso-Y	Aso-Y	–	4.0	0.1	E	91.4[d]
	Aso-ABCD	Aso-A Aso-B Aso-C Aso-D	SG06–5287	5.9	8.1	ENE	97.9 ± 6.0[b]
	Aso-EF	Aso-E Aso-F	–	5.2	1.7	E	99.2[d]
Stage 4	Aso-G	Aso-G	–	4.6	0.4	E	100.5[d]
	Aso-G'	Aso-G'	–	5.0	1.0	E	101.2[d]
	Aso-HI	Aso-H Aso-I	–	5.7	5.0	E	102.6[d]
	Aso-JKL	Aso-J Aso-K Aso-L	–	5.3	2.1	E	103.3[d]
	Aso-M	Aso-M	–	5.4	2.5	E	104.7[d]
Stage 3^	Aso-Z1 to 9	Aso-Z1 to 9	–	–	0.50 (total)	E	108.4–105.0[d]
Stage 2	Aso-10 to 26	Aso-10 to 26	–	–	1.20 (total)	ESE	114.1–108.4[d]
Stage 1	Aso-27 to 29	Aso-27 to 29	–	–	0.40 (total)	ESE	133.0–114.1[d]

1991; Miyabuchi, 2011). The ACP 6 to 3 fall units are all observed at Mizunomoto (Fig. 2) east of the caldera wall (Fig. 1D), and samples from this locality were subject to volcanic glass geochemical analysis (Albert et al., 2019a). Based on initial glass datasets the ACP3 glasses were easily distinguished at a major element level due to their higher SiO_2, and lower CaO contents relative to other post-caldera units previously analysed (Albert et al., 2019a). The ACP4 glasses can be distinguished from the ACP5 and ACP6 units as their glass compositions has had subtly higher SiO_2 contents, and have slightly higher Y content at a given Th content (Albert et al., 2019a). The glass of the older ACP5 and ACP6 tephra units showed considerable geochemical overlap and cannot be distinguish based on glass geochemistry alone (Albert et al., 2019a).

Above the ACP3 at the site of Mizunomoto (Fig. 1D; Fig. 2; Miyabuchi, 2011), there is a series of mafic scoria units that are interbedded between palaeosols, and are capped by the >1 m thick Kusasenrigahama pumice fall deposit (named Aso-Kpfa; Watanabe et al., 1982). The Aso-Kpfa is the largest and most voluminous pumice fall deposit from the post-caldera cones, it can be recognised in many outcrops around the Aso caldera (Miyabuchi, 2011), and has a bulk volume of 2.39 km^3, and corresponding to M5.1. It erupted from the Kusasenrigahama crater (Fig. 1D) and has six fall units, with dominant easterly and southern dispersals (Table 1). The Kpfa volcanic glass was previously characterised (McLean et al., 2020) to established a correlation to a cryptotephra deposit in Lake Suigetsu, SG14–2752. The Lake Suigetsu age-depth model (details below) provided an age of 32.7 ± 0.06 ka for the Kpfa eruption, which was consistent with previous age-estimates of the eruption and its close stratigraphic association with the 30 ka AT tephra (Fig. 2; Miyabuchi, 2009).

2.2. Pre-Aso-4 (ca. 130 ka – 86 ka)

At least thirty-seven eruption units are deposited between the caldera-forming Aso-3 (~130 ka) and Aso-4 (~86 ka) eruptions. The key units between these widespread marker layers, from oldest to youngest, include: Aso-N (Z2), Aso-M, Aso-JKL, Aso-HI, Aso-G', Aso-G, Aso-EF, Aso-ABCD and Aso-Y. These units have been grouped into five stages of activity according to magma composition and erupted volume (Table 1; Fig. 3, after Hoshizumi et al., 2022).

Several of these units have been successfully correlated with previously identified deposits identified by Ono and Watanabe (1983) and Ono et al. (1977), and here we have adopted the nomenclature outlined by Hoshizumi et al. (2022). The exception being the Aso-N (Z2) tephra which is stratigraphically equivalent to the previously reported Aso-N unit (see Hoshizumi et al., 2022) and, as it is discussed in the wider literature by both names, here we refer to this unit as Aso-N (Z2). Each tephra deposit typically consists of multiple fall units, representing individual phases of an eruption. Some of these tephra units are separated by poorly-developed palaeosols, which indicate time gaps between eruptive events. Additionally, interbedded with in the pre-Aso-4 tephrostratigraphy are key widespread marker tephras from other caldera volcanoes further south along the Ryukyu-Kyushu arc, specifically Ata (~100 ka, Ata tephra) and Kikai (~93 ka, K-Tz tephra) (Fig. 3). Detailed stratigraphic descriptions of these Aso units can be found in Hoshizumi et al. (2022). Here we provide a brief summary of the key physical and geochemical features of the different units.

Glass geochemistry has been published for the following selected pumice fall units: Aso-Y, Aso-ABCD (all sub-units), Aso-K, Aso-I, Aso-M and Aso-N (Z2), by Albert et al. (2019a). The glasses erupted from the oldest (Aso-N/Z2) and youngest (Aso-Y) pre-Aso-4 tephra deposits are distinctive from the glass compositions of the intervening deposits as they both have some of the highest K_2O content (~6.3 wt%) of all the Aso products, with the Aso-N (Z2) glasses classified as shoshonitic (Albert et al., 2019a). The Aso-M, Aso-K, Aso-I units all have similar major element glass chemistries, although the Aso-M glasses have subtly higher Sr contents. Moreover, these tephra deposits compositionally differ from the Plinian fall deposits stratigraphically above the Ata

tephra, Aso-ABCD (Albert et al., 2019a). The Aso-ABCD is the only eruption deposit where all fall units have been geochemically analysed and are broadly overlapping, although the lowermost Aso-D sub-unit has higher CaO contents relative to the other sub-units (Albert et al., 2019a). Trace elements can further geochemically distinguish the Aso-ABCD sub-units; Aso-B and Aso-C have lower levels of enrichment (e.g. Th content), compared to those of Aso-A and Aso-D (Albert et al., 2019a).

The Aso-3 eruption is the penultimate caldera-forming eruption; its age is loosely constrained between ca. 123–130 ka (Nagahashi et al., 2004a, 2004b; Chun et al., 2004; Machida and Arai, 1994). This eruption produced a Plinian fall and PDC deposits, with a bulk volume of more than 180 km^3 (Hoshizumi et al., 2024; Ono et al., 1977). The tephra fall is observed across a wide regional area of southwestern and central Japan, and thus is a prominent marker layer (e.g., Machida and Arai, 1994, 2003), and it provides the lowermost tephrostratigraphic constraint for this study.

Hoshizumi et al. (2022) divided Aso's eruptive activity after the Aso-3 eruption into distinct stages based on changes in eruption frequency, magma composition, and dispersal characteristics. This classification helps distinguish phases of more frequent, small-scale mafic eruptions from less frequent but larger silicic eruptions, providing a clearer framework for understanding Aso's long-term volcanic evolution. Following the Aso-3 eruption, there was relatively frequent eruptive activity, comprised of small eruptions that produced mafic scoria and ashfall, during Stages 1 (133.0–114.1 ka) and 2 (114.1–108.4 ka), before more silicic eruptions occurred in Stage 3 (108.4–104.7 ka; Hoshizumi et al., 2022). These three stages of activity only erupted a collective total bulk volume of 2.1 km^3 across an ~28 kyr period, and their dispersals are considered to be limited with E-SE trajectories (Table 1; Fig. 3; after Hoshizumi et al., 2022). The more silicic tephra units erupted during Stage 3 are composed of nine pumice- and ash-fall eruptions (Aso-Z9 to Z3, Aso-N [Z2], and Z1), that are all considered M3 to 4, and they are interbedded between palaeosols at Katayama (Table 1; Fig. 3). Hoshizumi et al. (2022) note that the Aso-Z6 (a 27 cm thick alternating pumice- and ash fall unit) and the Aso-N (white pumice fall layer) tephra units are the most useful Stage 3 marker layers as they are frequently observed in outcrops to the east of the caldera rim (Fig. 3). The Aso-N (Z2) pumice fall glass has been previously analysed, these high-SiO_2 Aso rhyolites (73 wt%) show distinctive levels of incompatible trace element enrichment, with Th contents (~25 ppm) far exceeding all other Aso units characterised previously (Albert et al., 2019a).

The most active phase between Aso-3 and Aso-4 was Stage 4 that based on existing chrono-stratigraphy spanned 7 kyrs (104.7–97.7 ka; Hoshizumi et al., 2022). Stage 4 includes at least seven tephra units composed of numerous layers pumice lapilli and ashfall layers that are separated by well-developed soils. These Stage 4 tephra units are: Aso-M, Aso-JKL, Aso-HI, Aso-G', Aso-G, Aso-EF and Aso-ABCD (Fig. 3; Hoshizumi et al., 2022). The Aso-J sub-unit of Aso-JKL, Aso-G', Aso-G and Aso-E have only recently been classified by Hoshizumi et al. (2022), while the others are more prominent deposits (see: Ono and Watanabe, 1983; Ono et al., 1977). The Stage 4 eruptions each produced bulk volumes ranging from 0.4 to 8.1 km^3 corresponding to M4.6 to M5.9 (Table 1; Hoshizumi et al., 2022). The oldest of these tephra deposits (Aso-M) is a 3 m thick unit at Katayama (see Fig. 3), which is comprised of stratified black ash and white pumice layers, although there is evidence of erosional contact in the base of the upper-ash layer, indicating that deposit may reflect different eruptions separated in time (Hoshizumi et al., 2022).

Hoshizumi et al. (2022) identified the Aso-J sub-unit and interpreted it to be part of the Aso-KL eruption/tephra, as defined by Ono and Watanabe (1983), and considered the bulk volume of Aso-JKL eruption to be 2.1 km^3 (Table 1). At the site of Katayama, the Aso-JKL tephra is found directly above a ~ 0.5 m thick soil separating it from the underlying Aso-M unit (Fig. 3). The lowermost Aso-L unit is 0.7 m thick and comprises alternating layers of ash and pumice, which is overlain by the 0.7 m thick, white pumice layer of Aso-K unit. These are followed by the much thicker ~2 m thick Aso-J unit, which is comprised of alternating pumice lapilli and ash-layers (Fig. 3). Hoshizumi et al. (2022) observe that as you move east and away from the caldera, the smaller Aso-J and Aso-L sub-units are often unclear or absent (i.e. Noga, Numerize and Tsuru; Fig. 3),.

Above the Aso-JKL tephra at the site of Katayama (Fig. 1D), there is a 0.3 m weathered ash layer followed by the 8.0 m thick Aso-HI tephra (Fig. 3). The estimated volume of the Aso-HI eruption is 5.0 km^3, making it the second largest eruption between the Aso-3 and Aso-4 eruptions, and it is considered to have a dominant easterly dispersal (Table 1; Hoshizumi et al., 2022). The lower Aso-I sub-unit is a ~ 2.5 m thick pumice lapilli layer, whilst the Aso-H sub-unit is a ~ 5.5 m thick sequence of alternating layers of pumice lapilli and ash fall (Fig. 3). Previously only the volcanic glasses of the lowermost Aso-I fall unit from Noga were geochemically characterised (Albert et al., 2019a).

The Aso-G' and subsequent Aso-G tephra units have only recently been identified by Hoshizumi et al. (2022), and are most prominent at the site of Hinatame (Fig. 1), 11 km to the east of the caldera wall. These two units have not yet been identified in other sequences further northeast (Fig. 3). At the site of Hinatame (Fig. 1D), the lower Aso-G' eruption is a ~ 1.0 m thick dark grey ash layer, and dispersed 1.0 km^3 of tephra to the SE. The overlying Aso-G tephra sits upon a well-developed soil, and consists of three pumice lapilli layers. The estimated volume of Aso-G is 0.4 km^3 and it was dispersed along a more easterly trajectory (Fig. 3; Hoshizumi et al., 2022). Neither the Aso-G' or the Aso-G tephra deposits have had their glass geochemically characterised.

Above a well-developed soil, is the Aso-EF tephra that has a bulk volume of 1.7 km^3 (Ono and Watanabe, 1983; Ono et al., 1977). It is frequently identified in outcrops beyond the caldera wall, and is clearly preserved at the site of Hinatame (Fig. 3; Hoshizumi et al., 2022). The older Aso-F is 0.5 m thick pumice lapilli fall unit, whilst the overlaying Aso-E unit is a ~ 1.5 m thick stratified ash layers with several thin pumice lapilli layers throughout, while the degree of stratification diminishes with increasing distance from the caldera (Fig. 3; Hoshizumi et al., 2022).

The youngest of the Stage 4 tephras is the Aso-ABCD eruption that is comprised of Plinian fall units, and represents the largest eruption (M5.9) between Aso-3 and Aso-4, erupting 8.1 km^3 of trachytic-dacite to predominantly rhyolitic tephra (Hoshizumi et al., 2022; Albert et al., 2019a; Smith et al., 2013). The Aso-ABCD tephra is preserved between Ata and K-Tz marker layers in proximal settings (e.g, at Noga; Fig. 3), and the units are pumice lapilli fall deposits except for the thinner Aso-B unit which is an ash-fall layer (Fig. 3). The Aso-ABCD measures 4.3 m in thickness at Noga, where the Aso-D and Aso-A are the thickest units (Fig. 3). The Aso-ABCD sub-units have subtly different glass compositions, and thus, the 3.5 cm thick visible SG06–5287 tephra layer preserved in Lake Suigetsu has been tentatively correlated to the Aso-A sub-unit of the Aso-ABCD eruption. This correlation provides an age of 96.8 ± 2.6 ka for the Aso-ABCD eruption (Albert et al., 2019a), which is in good agreement with the 97.7 ka age estimated based on the chrono-stratigraphy of the TKN-2004 core Nagano, central Japan (Nagahashi et al., 2007).

Only one eruption deposit, Aso-Y, occurs in the Stage 5 interval between Aso-4 and Aso-ABCD (97.7–88.0 ka; Hoshizumi et al., 2022). This represents a significant drop in the eruption frequency, with just the single pumice-fall (Aso-Y) deposit recognised in the 10 kyrs prior to the Aso-4 caldera-forming eruption (Table 1; Hoshizumi et al., 2022). The abrupt drop in eruption frequency is thought to be a typical characteristic of the evolution of a magmatic system in the fermentation phase of a caldera cycle (Keller et al., 2023; Hoshizumi et al., 2022; de Maisonneuve et al., 2021). The Aso-Y tephra is not widely traced in the near-source area, thus has a relatively small volume estimate of ~0.1 km^3, measuring just 0.2 m thick white pumice lapilli at Noga. Aso-Y is also recognised Hinatame and Kurumibaru (Fig. 3). The layer is found stratigraphically above the widespread K-Tz marker from the Kikai caldera located ~300 km south of Aso (Fig. 3; Hoshizumi et al., 2022).

The rhyolitic volcanic glasses of the Aso-Y pumices from Noga have previously been geochemically characterised by Albert et al. (2019a).

At the site of Kurumibaru (Fig. 1D), stratigraphically above the Aso-Y tephra and a soil, is a 3.0 m thick white pumice lapilli fall deposit, named the Aso-4X (Fig. 3). This recently discovered unit is directly overlain by Aso-4 PDC deposits (Fig. 3; Hoshizumi et al., 2022) and is considered to be the initial Plinian phase of the Aso-4 caldera-forming eruption (Hoshizumi et al., 2022). The glasses of the Aso-4X fall deposit have not been previously analysed, but the Aso-4 PDC deposits are distinctive owing to their compositional heterogeneity. The proximal glasses from PDC deposits at Noga reveal three distinct glass populations, with two dominant rhyolitic populations which have different CaO, and FeOt contents (see Albert et al., 2019a). The glass chemistry of the 3.5 cm thick visible tephra preserved in Lake Suigetsu (SG06–4963) shows good geochemical agreement with the two rhyolitic components of the Aso-4 glasses (Smith et al., 2013).

As previously mentioned, the massive M8.0–8.4 Aso-4 eruption is the second largest volcanic event experienced on Earth within the last 100 kyr, and is the largest of the Aso caldera-forming eruptions (Albert et al., 2019a; Takarada and Hoshizumi, 2020; Keller et al., 2023). The pyroclastic density currents (PDC) deposits of Aso-4 are found up to 50 km beyond the caldera wall (Hoshizumi et al., 2022; Takarada and Hoshizumi, 2020), and fallout is reported in terrestrial and marine cores across in and around Japan (e.g. Matsu'ura et al., 2021; Tsuji et al., 2018; Lim et al., 2013; Smith et al., 2013; Nagahashi et al., 2004a, 2004b). During the eruption >900 km ^{3} of tephra was ejected and dispersed over wide areas (Takarada and Hoshizumi, 2020).

3. Methods

3.1. Proximal tephra samples

With a view to supplementing existing Aso glass datasets (outlined above) we collected tephra samples from outcrops where the stratigraphy is well established (e.g., Miyabuchi et al., 2003; Miyabuchi, 2009; Hoshizumi et al., 2022). All of the sections have been previously studied and are located east, north-east and south-east of the caldera wall (Fig. 1D). During field campaigns in 2022 and 2023, we targeted silicic eruption deposits, tephra beds were comprised of pumice lapilli and ash fall beds, that are positioned between Aso-3 (~123–130 ka) and the widespread AT tephra (30 ka). In the pre-Aso-4 interval the nomenclature and stratigraphy of Hoshizumi et al. (2022) was followed at Noga, Katayama and Kurumibaru sites (Fig. 1D; Fig. 3). A fourth section, Hata, was also additionally sampled, and stratigraphically correlated into the aforementioned sections using the stratigraphy and deposit characteristics (Fig. 3). Across the investigated sequences and below the Aso-4 PDC, eleven Aso eruptions were targeted for volcanic glass chemical analysis from interval, Aso-Z6, Aso-N (Z2); Aso-M, Aso-JKL, Aso-HI, Aso-G' Aso-G, Aso-EF, Aso-ABCD, Aso-Y, and Aso-4X. Glass analysis of our Aso-G' sample was unsuccessful.

Post- Aso-4 sampling of the eruption units followed the stratigraphic framework of Miyabuchi et al. (2003), Miyabuchi (2009, 2011), with samples collected for analysis at four outcrops, Nojiri, Yamasaki, Koga and Takimizu (Fig. 1D; Fig. 2). These samples supplement previous post-Aso-4 samples collected from Mizunomoto (site A9831; Miyabuchi, 2009), and their glass data are reported by Albert et al. (2019a). Across the investigated localities and above the Aso-4 PDC, the deposits of at least ten eruptions were targeted for new chemical analysis, these include the: NjP, YmP8, YmP7, YmP6, YmP5, ACP6, ACP4, ACP3, Kpfa and a post-Kpfa ash bed.

The 2022/23 samples collected for geochemical analysis were given a number and a FLF prefix, while those collected in previous field campaigns retain the prefix associated with earlier field sampling campaigns (e.g., A9746 - YmP5; Miyabuchi, 2011; or ITJ207; Albert et al., 2019a). In the laboratory, these bulk representative samples of pumice clasts and ash were crushed and wet sieved, removing the fraction <25 μm. Samples were oven dried at ~60 °C and then mounted in Struers Epoxy resin. The surfaces of the resin stubs were manually sectioned using silicon carbide papers to expose the shards on a flat surface, samples were polished with using polishing pads embedded with diamond paste (3 and 1 μm), and then carbon coated for chemical analyses.

3.2. Geochemical analysis (Volcanic glass)

Major element compositions of individual glass shards were analysed using a JEOL JXA-8200 wavelength dispersive electron microprobe (WDS-EMP) equipped with 5 spectrometers located in the School of Archaeology, University of Oxford, U.K. An accelerating voltage of 15 kV, 6 nA current and a defocussed 10 μm beam were used. Peak counting times were 12 s for Na, 30 s for other major elements except for Mn, Cl and P, which were collected for 50 s. A suite of mineral standards were used to calibrate the microprobe, and the MPI-DING references glasses (Jochum et al., 2006) were run as secondary standards during each analytical session. A subset of samples were analysed using a Cameca SX100 WDS-EMP with five wavelength dispersive spectrometers at the Tephra Analytical Unit, University of Edinburgh. Analyses were conducted at an accelerating voltage of 15 kV, with a beam current of 2 nA for higher abundance elements (Al, Si, Fe, K, Ca, Na, Mg), while 80 nA for those with typically lower abundances (Mn, Cl, P, Ti). All glasses were analysed using the 5 μm beam set-up as outlined in Hayward (2012). Peak counting times were 20 s for all elements except Ti (30s), Fe (40s), Mn (50s). Pure metals, synthetic oxides and silicate standards were used for calibration as outlined in Hayward (2012). The secondary Lipari and BCR2g standards were analysed at regular intervals, alongside the MPI-DING glasses. Analyses with analytical totals <93 % were discarded. All analyses presented have been normalised to 100 % for comparative purposes.

The trace element compositions of the individual volcanic glasses were determined by Laser Ablation Inductively Coupled Plasma Mass Spectrometry (LA-ICP-MS). The analyses were conducted using a Agilent 8900 triple quadrupole ICP-MS (ICP-QQQ) coupled to a Resonetics 193 nm ArF excimer laser-ablation device in the Department of Earth Sciences, Royal Holloway, University of London. Both 20 and 25 μm crater sizes were used depending on the size of the exposed glass surface area. The laser energy density on the target was 3.0 Jcm^{-2}, the repetition rate was 5 Hz. Ablation of the samples lasted 40 s on the sample, while 20 s of pre- and 20 s of post-ablation gas blank was used to subtract the background signal. The MPI-DING reference glasses were used to monitor analytical accuracy (Jochum et al., 2006). Typically, blocks of eight glass shards and one MPI-DING reference glass were bracketed by the NIST612 glass adopted as the calibration standard. The internal standard applied was ^{29}Si (determined by WDS-EMP analysis). LA-ICP-MS data reduction was performed in Microsoft Excel, following the protocols described in Tomlinson et al. (2010). Accuracies of LA-ICP-MS analyses were monitored using MPI-DING reference glasses, ATHO-G and StHs6/80-G, and were typically ≤5 % for most elements measured (see Supplementary Material). Error bars on plots represent reproducibility, calculated as ±2 standard deviations of replicate analyses of MPI-DING StHs6/80-G glasses. All secondary standards analyses from the EMP and LA-ICP-MS run alongside Aso samples, can be found in the Supplementary Material.

3.3. Chronology of the Lake Suigetsu crypto−/tephra deposits from Aso

In this study, the compositional data for all twenty Aso-derived Lake Suigetsu tephra layers (see Vineberg et al., 2024; McLean et al., 2020; Albert et al., 2019a; Smith et al., 2013) were compared to the new glass geochemical data for the near-source eruption deposits sampled here, and published data, to facilitate proximal-distal correlations.

Correlations to the tephra layers preserved in the Lake Suigetsu sediments allow the age-model to be used to provide ages for the eruptions preserved within the sediments. Critically, SG06 event-free

depth(s) (EFD; version 13th Feb 2017) were used within the age model, which excludes instantaneous deposits >5 mm in thickness, i.e., event layers (Staff, R.A et al., 2011; Schlolaut et al., 2012). The software package developed to handle the correlation of parallel core sections, 'LevelFinder' (version 7.7.1, http://polsyems.rits-paleo.com), was used to linearly interpolate between the common marker layers to determine a composite depth (CD) or EFD for the cryptotephra layers. Up to the limit of radiocarbon dating (circa 52 cal. ka BP), the Lake Suigetsu age-depth model is derived directly from the integration of its radiocarbon (^{14}C) and varve datasets into the composite consensus international radiocarbon calibration curve, IntCal20 (Bronk Ramsey et al., 2020; Reimer et al., 2020). For the deeper section of the stratigraphy examined in the present study, this chronology was extrapolated using a 'P_Sequence' deposition model within the Bayesian software package, OxCal (Bronk Ramsey, 2008), and includes the ^{40}Ar/^{39}Ar-derived age of 86.4 ± 0.6 ka (±1σ) for the Aso 4 tephra which is identified at a CD in SG14 of 4922.8 cm (Albert et al., 2019a; see below). The Lake Suigetsu age model-derived ages (ka) for the tephra identified in this section are reported in Table 2 and the ±1σ uncertainties are quoted.

4. Results

The glass chemistry of twenty recognised silicic eruptions (pumice and ash fall), 10 pre- and 10 post- Aso-4, are presented from sequences between the Aso-3 and the AT tephra at sites located to the east, north-east and south-east of the Aso caldera wall (Figs. 2 and 3). Many of these eruptions have multiple eruptive phases (sub-units), as such forty-five samples spanning 20 eruption deposits were analysed to attempt to capture the full chemical variability of the individual eruptive units. Selected major and trace element analyses are reported in Table 2; while the full glass geochemical dataset is provided in the Supplementary Material.

The composition of the Aso glasses typically straddle the trachydacite – rhyolite boundary with SiO_2 ranging from 65.5 to 74.6 wt% and $N_2O + K_2O$ ranging from ~8.3 to 9.9 wt% (Fig. 4A). The YmP7 and YmP6 are exceptions, having glasses that are less evolved with SiO_2 ranging from 58.5 to 64.2 wt% and $Na_2O + K_2O$ from 6.4 to 8.1 wt%, thus extending from trachy-andesite to trachyte (Fig. 4A). The majority of Aso units analysed have a High-K calc-alkaline affinity with K_2O contents ranging from ~3 wt% at 58 wt% SiO_2 to ~5 wt% at 73 wt% SiO_2. Aso-N (Z2) is unique in that its glasses display higher K_2O content (6 wt% at 73 wt% SiO_2) giving it a shoshonitic affinity. Collectively, many of the Aso units have overlapping major element glass compositions (Fig. 4; Table 2), and individual eruptions and phases can be difficult to discriminate using major element compositions alone (Fig. 4A). Many of the analysed deposits are homogeneous with the chemical ranges of individual units being similar to analytical uncertainty., The only exceptions being Aso-I, Aso-F, and YmP6 which show higher degrees of compositional variability at a major element level (Fig. 4A; Table 2). The trachytic glasses of the YmP5 appear to be largely distinct from all other units analysed (Fig. 4A).

Trace element data has been obtained for eighteen of the sampled units (Table 2). However, some tephra deposits were not analysed due to poor preservation of the volcanic glass prohibiting identification of glass surface adequately large enough for 20 μm spot analysis (e.g., the NjP). There is considerable overlap in the incompatible trace element concentrations of many of the eruption deposits analysed (Fig. 4B-C). The Zr – Th ratios are broadly constant within the entire suite of near-source glasses analysed (Fig. 4B) with the greatest variability observed in the post-Aso-4 units, largely a function of elevated values associated with the ACP4 and ACP6 products (Fig. 4B). In general, the different eruption deposits are often more easily distinguishable using trace elements, for instance Sr. Significant variations can be observed in the Sr content (667 to 47 ppm) of the Aso volcanic glasses analysed here through the entire post-Aso-3 tephra sequence (Fig. 4C). As indicated by their less evolved major element compositions, the YmP5 to 8 tephra units analysed retaining higher Sr content (>320 ppm) than the other units analysed (Fig. 4B). Again, the Aso-F glasses show heterogenous compositions at the trace element level, with Th content ranging from 13.2 to 24.2 ppm, and displaying a unique cluster of glasses at ~24 ppm Th (Fig. 4B). The highest SiO_2 glasses of the Aso-N (Z2), ACP6 and ACP3 glasses display the lowest Sr contents (<100 ppm) when compared to other Aso units, which may be a useful distinguishing feature of the glasses of these eruptions (Fig. 4B). Below we highlight the key compositional features of the near source units, and compare them to previously published datasets, to reveal the potentially diagnostic chemical features, which in conjunction with a robust tephrostratigraphic framework can be used to aid tephra correlations.

4.1. Post-Aso-4

The homogeneous rhyolitic (SiO_2 = 69.4 ± 0.3 wt%; $Na_2O + K_2O$ = 9.2 ± 0.2; 1σ; *n = 18*) glasses of the Aso-Kpfa tephra sampled at Takimizu are consistent with previously published data for the unit (McLean et al., 2020; Fig. 5A). The ash bed above the Aso-Kpfa identified and characterised here can easily be distinguished from the Aso-Kpfa tephra as the younger ash has a trachytic glass composition, with lower SiO_2 (64–67 wt%) and higher CaO content (3.4–2.7 wt%) contents (Fig. 5A).

At Takimizu (ENE of the caldera) the ACP3 glasses are homogenous rhyolites (SiO_2 = 74.0 ± 0.3; CaO = 0.7 ± 0.1 wt% [1σ; *n = 17*]), while the ACP4 volcanic glasses at the site are predominantly less evolved rhyolites (SiO_2 = 71.9 ± 0.6 wt%; CaO = 1.19 wt% [*n = 46*]; Fig. 5A). The Takimizu glass data from the ACP3 and ACP4 deposits are consistent with previously published data from Mizunomoto (Fig. 5A). NE of the caldera wall at Koga, the ACP4 rhyolitic glasses (SiO_2 = 71.7 ± 1.3 wt%; CaO = 1.5 ± 0.3 wt%; [1σ, *n = 23*], Fig. 5A) are broadly consistent with those from ACP4 deposits at Takimizu and Mizunomoto (Fig. 5A). However, at the trace element level, the Lower ACP4 pumice fall (FLF191) and the Upper pumice fall (FLF192) can be discriminated, with the lower pumices being more depleted in Sr (132–113 ppm) at overlapping Th content, relative to the overlying ACP4 upper pumice layer (Sr = 194–158 ppm; Fig. 5B). A bulk ACP4 sample (FLF190) collected encompassing the entire ACP4 sequence at Koga contains both Sr populations. The discrete Sr populations in the Koga pumice beds is not seen in the data from Takimizu or Mizunomoto E of the caldera, where the Sr contents are consistent with the upper Koga pumice glasses (Fig. 5D). The glass data from Koga reveals that two phases of the ACP4 eruption deposit can be distinguished at the trace element level (Sr), which has not previously been observed (Fig. 5B).

With regards to the glass compositions of the ACP6 deposits, the basal pumice fall sampled from Koga (NE of the caldera) is compositionally distinct from the previously published ACP6 glass data from Mizunomoto E of the caldera wall (Albert et al., 2019a). The basal Koga ACP6 pumice fall unit is dominated by a higher SiO_2 (72.7 ± 1.16 wt% [1σ, *n = 21*]) and lower CaO (ca. 0.7 wt%) content rhyolitic glasses, which are considerably more evolved than those of the thickest upper ACP6 pumice fall deposit sampled at Mizunomoto, where ~69–71 wt% SiO_2 glasses dominate (Fig. 5A-B). Furthermore, the laterally discontinuous upper ACP6 pumice fall at Koga are more heterogenous rhyolites (SiO_2 = 68.6–73.6 wt%; *n = 14*) and shows the volcanic glass compositions consistent with both the Lower Koga ACP6 fall and the Upper Mizunomoto fall (Fig. 5A-B). Although the previously published data indicated that the most silicic ACP deposits were those of the ACP3 eruption, and were distinguishable from ACP4–6. The data here for ACP6 reveals a partial overlap with the highly evolved ACP3 rhyolitic glass compositions (Fig. 5A-B).

With regards to the Yamasaki Pumice (YmP) series erupted between ca. 61–77 ka as described by Miyabuchi (2009), the four fall deposits analysed here (YmP5, YmP6 YmP7 and YmP8) reveal a broad SiO_2 range from trachy-andesite to trachyte (58–68 wt% SiO_2; Fig. 4A). These four units are easily distinguishable from other Aso units using major and/or trace element compositions owing to being less evolved (Fig. 4A-C). The

Table 2

Average major (EMP) and trace element (LA-ICP-MS) volcanic glass chemistry of the of the proximal Aso units sampled between Aso-3 and the AT marker beds. Major element glass data has been normalised. Sampling locations are shown in Fig. 1D. Full geochemical datasets are available in the Supplementary Material, along with the coordinates of the sampled localities.

Tephra	Post Kpfa ash		Aso-Kpfa		ACP3		ACP4		ACP4		ACP4		ACP4		ACP4 (Lower)		ACP4 (Upper)		ACP6 (Lower)		ACP6 (Upper)		YmP5		YmP6		YmP7		YmP8	
Material	Ash		Pumice		Pumice		Pumice		Pumice		Pumice		Pumice		Pumice		Pumice		Pumice		Pumice		Pumice		Pumice		Ash		Pumice	
Sample id	FLF57		FLF56		FLF58		FLF60		FLF61		FLF62		FLF63		FLF190		FLF191		FLF186		FLF187		A9746 P-B4		P-B5/4		P-B5		A9746 P-B6	
Location	Takimizu (0822_27)		Takimizu (0822_27)		Takimizu (0822_27)		Takimizu (0822_27)		Takimizu (0822_27)		Takimizu (0822_27)		Takimizu (0822_27)		Koga (0923_07)		Koga (0923_07)		Koga (0923_07)		Koga (0923_07)		Yamasaki (A9746)		Yamasaki (A9746)		Yamasaki (A9746)		Yamasaki (A9746)	
(wt.%)	Avg.	1σ	Avg.	1σ	Avg.	1σ	Avg.	1σ	Avg.	1σ	Avg.	1σ	Avg.	1σ	Avg.	1σ	Avg.	1σ	Avg.	1σ	Avg.	1σ	Avg.	1σ	Avg.	1σ	Avg.	1σ	Avg.	1σ
SiO_2	66.01	1.04	69.40	0.33	74.04	0.27	71.89	0.16	71.94	0.48	71.91	0.97	72.18	0.94	71.71	0.51	72.49	1.68	72.70	1.16	72.05	1.93	65.96	0.64	61.89	4.05	61.12	0.40	68.03	0.36
TiO_2	0.91	0.03	0.73	0.02	0.33	0.03	0.45	0.02	0.47	0.06	0.45	0.08	0.43	0.08	0.48	0.12	0.43	0.13	0.36	0.13	0.46	0.20	0.73	0.04	0.88	0.25	0.91	0.03	0.65	0.04
Al_2O_3	15.12	0.21	15.05	0.20	14.00	0.21	14.99	0.10	14.95	0.21	14.89	0.39	14.79	0.38	14.86	0.08	14.54	0.97	14.57	0.44	14.55	0.46	16.10	0.52	16.41	1.45	16.69	0.33	15.87	0.28
FeO	4.63	0.35	2.74	0.13	1.24	0.06	1.69	0.05	1.71	0.14	1.70	0.26	1.69	0.22	1.75	0.24	1.42	0.54	1.47	0.42	1.88	0.78	4.01	0.37	6.13	2.37	6.30	0.20	3.08	0.15
MnO	0.13	0.01	0.11	0.01	0.07	0.03	0.09	0.03	0.07	0.01	0.08	0.02	0.07	0.02	0.08	0.02	0.07	0.06	0.07	0.03	0.08	0.02	0.16	0.04	0.16	0.07	0.17	0.02	0.12	0.02
MgO	1.17	0.14	0.66	0.03	0.19	0.02	0.38	0.04	0.34	0.05	0.38	0.09	0.34	0.08	0.36	0.05	0.39	0.38	0.27	0.14	0.38	0.24	1.27	0.60	1.97	1.04	2.14	0.11	0.78	0.12
CaO	3.01	0.30	1.88	0.05	0.68	0.05	1.22	0.03	1.17	0.13	1.18	0.25	1.11	0.23	1.20	0.20	0.98	0.43	0.83	0.36	1.10	0.57	3.02	0.26	4.72	1.62	4.87	0.23	2.31	0.17
Na_2O	4.56	0.12	4.86	0.13	4.27	0.09	4.57	0.10	4.60	0.16	4.53	0.17	4.61	0.19	4.71	0.14	4.59	0.45	4.47	0.21	4.51	0.15	4.54	0.17	4.05	0.53	4.11	0.19	4.38	0.13
K_2O	4.09	0.06	4.35	0.06	5.04	0.08	4.55	0.08	4.60	0.14	4.66	0.24	4.63	0.23	4.70	0.14	4.98	0.57	5.08	0.34	4.83	0.42	3.88	0.22	3.27	0.80	3.08	0.14	4.52	0.15
P_2O_5	0.29	0.05	0.11	0.01	0.02	0.01	0.05	0.02	0.05	0.02	0.05	0.03	0.04	0.02	0.06	0.06	0.05	0.02	0.05	0.04	0.05	0.05	0.24	0.09	0.44	0.18	0.51	0.06	0.16	0.02
Cl	0.08	0.01	0.11	0.04	0.11	0.01	0.11	0.02	0.10	0.01	0.10	0.01	0.10	0.01	0.10	0.03	0.06	0.04	0.12	0.02	0.11	0.03	0.10	0.01	0.08	0.04	0.08	0.01	0.10	0.01
(n)	6		19		17		15		12		13		6		9		6		21		14		14		15		17		13	
(ppm)	Avg.	1σ	Avg.	1σ	Avg.	1σ	Avg.	1σ	Avg.	1σ	Avg.	1σ	Avg.	1σ	Avg.	1σ	Avg.	1σ	Avg.	1σ	Avg.	1σ	Avg.	1σ	Avg.	1σ	Avg.	1σ	Avg.	1σ
V					13.3	1.1	20.9	0.6	20.7	1.3	21.5	1.4	18.5	5.7	19.0	0.4	21.3	2.7	16.8	11.5	22.9	17.6	23.8	1.6	146.1	101.3	79.8	13.8	25.6	1.9
Pb	-	-	-	-	174	3	155	4	151	6	154	3	146	20	161	6	149	2	165	11	154	22	140	7	113	9	113	4	165	4
Sr	-	-	-	-	66	7	151	3	155	16	154	13	201	157	123	7	174	14	109	51	158	122	455	82	519	70	522	30	356	11
Y	-	-	-	-	35.6	1.0	35.8	0.9	34.7	0.9	35.1	1.0	34.3	2.9	35.1	0.5	35.5	2.0	35.5	0.8	34.0	1.2	30.3	1.9	29.0	2.6	28.1	2.1	31.2	1.4
Zr	-	-	-	-	298	15	301	11	293	11	300	9	275	23	310	7	299	12	308	22	296	39	233	14	186	16	190	16	286	12
Nb	-	-	-	-	17.5	0.4	17.1	0.4	16.9	1.0	16.7	0.3	16.1	1.5	17.0	0.3	16.3	0.5	16.7	0.7	16.0	1.0	12.6	0.7	10.0	0.6	9.9	0.6	15.1	0.5
Ba	-	-	-	-	760	28	828	14	810	29	838	22	790	59	799	29	774	49	785	50	733	59	737	29	594	36	607	38	852	50
La	-	-	-	-	33.3	1.0	33.1	1.3	32.3	0.7	33.6	1.0	32.5	1.8	32.1	0.7	31.6	0.6	33.0	0.8	31.8	1.3	28.8	1.3	25.7	1.7	25.8	2.2	31.8	1.3
Ce	-	-	-	-	72.6	2.5	71.1	2.5	69.9	4.3	72.0	2.5	70.8	4.4	70.6	2.0	70.0	1.4	72.2	2.8	68.6	3.1	63.3	3.2	57.3	5.0	59.6	6.2	69.1	6.6
Pr	-	-	-	-	8.6	0.2	8.4	0.3	8.4	0.3	8.5	0.4	8.2	0.7	8.3	0.2	8.4	0.3	8.4	0.3	8.1	0.4	7.65	0.7	7.01	0.5	6.97	0.8	8.03	0.2
Nd	-	-	-	-	34.6	1.3	34.7	1.1	33.9	1.8	34.6	1.7	33.6	1.9	34.2	0.7	33.7	1.0	34.4	1.3	33.6	1.7	32.0	1.8	30.7	2.8	31.5	2.6	33.1	1.0
Sm	-	-	-	-	7.3	0.3	7.2	0.4	7.5	0.6	7.3	0.5	6.7	0.6	7.2	0.3	7.1	0.8	7.4	0.4	7.3	0.1	7.02	0.4	6.91	0.8	7.37	0.6	7.58	0.8
Eu	-	-	-	-	1.4	0.1	1.7	0.1	1.8	0.6	1.4	0.1	1.4	0.3	1.3	0.1	1.5	0.1	1.3	0.2	1.3	0.3	1.66	0.2	1.69	0.1	1.80	0.2	1.56	0.1
Gd	-	-	-	-	6.1	0.3	6.3	0.5	6.2	0.3	6.2	0.3	6.0	0.2	6.2	0.4	6.5	0.1	6.4	0.4	6.3	0.1	5.96	0.8	5.81	0.4	5.92	0.7	5.85	0.5
Dy	-	-	-	-	6.1	0.3	6.3	0.4	5.8	0.5	6.2	0.4	5.9	0.6	6.2	0.4	6.2	0.5	6.4	0.3	6.2	0.2	5.47	0.5	5.30	0.5	5.27	0.8	5.50	0.4
Er	-	-	-	-	3.9	0.3	3.8	0.2	3.6	0.3	3.8	0.1	3.8	0.5	3.8	0.2	3.9	0.3	4.0	0.3	3.8	0.2	3.35	0.3	3.15	0.3	2.96	0.3	3.59	0.3
Yb	-	-	-	-	4.2	0.3	4.2	0.3	4.1	0.2	4.2	0.3	4.0	0.3	4.2	0.3	4.2	0.1	4.2	0.2	4.1	0.5	3.35	0.4	3.07	0.3	3.16	0.3	3.64	0.5
Lu	-	-	-	-	0.65	0.05	0.62	0.03	0.58	0.03	0.61	0.02	0.61	0.06	0.63	0.03	0.62	0.05	0.63	0.03	0.61	0.05	0.50	0.05	0.46	0.05	0.45	0.06	0.50	0.04
Hf	-	-	-	-	8.0	0.6	8.0	0.6	7.5	0.3	8.0	0.3	7.4	0.6	8.5	0.5	8.0	0.5	8.3	0.8	7.9	1.3	6.17	0.5	5.13	0.5	4.86	0.6	6.94	0.8
Ta	-	-	-	-	1.3	0.1	1.2	0.1	1.1	0.1	1.2	0.0	1.1	0.1	1.2	0.1	1.2	0.0	1.2	0.1	1.2	0.2	0.90	0.1	0.71	0.1	0.71	0.1	1.09	0.1
Pb	-	-	-	-	24.3	0.8	22.7	1.0	22.7	1.3	23.6	1.1	22.8	2.2	24.3	1.1	21.9	1.1	24.5	1.6	22.4	0.7	20.8	2.1	16.9	1.6	16.2	1.5	23.0	1.0
Th	-	-	-	-	16.1	0.9	14.2	0.8	13.4	0.7	14.7	0.6	14.3	1.8	14.5	0.5	14.3	0.6	15.8	1.5	14.8	2.9	12.6	0.8	10.3	1.0	10.1	1.4	15.5	1.4
U	-	-	-	-	4.7	0.2	4.1	0.3	4.0	0.1	4.2	0.1	4.1	0.5	4.3	0.1	4.2	0.2	4.5	0.4	4.2	0.6	3.70	0.2	2.96	0.4	3.08	0.3	4.51	0.3
(n)	-		-		13		7		8		7		4		5		5		16		4		11		8		10		10	

(*continued on next page*)

Table 2 (*continued*)

Tephra	NjP		Aso-4X (lower)		Aso-4X (middle)		Aso-4X (upper)		Aso-Y		Aso-Y		Aso-D		Aso-E		Aso-E (lower)		Aso-E (middle)		Aso-E (upper)		Aso-F		Aso-F		Aso-G		Aso-H (base)	
Material	Ash		Pumice		Pumice		Pumice		Pumice		Ash		Pumice		Pumice		Pumice		Ash		Ash		Pumice		Pumice		Pumice		Pumice	
Sample id	FLF52		FLF194		FLF195		FLF196		FLF65		FLF248		FLF236		FLF74		FLF232		FLF233		FLF234		FLF73		FLF230		FLF229		FLF208	
Location	Njori (0822_26)		Kurumibaru (AS10042)		Kurumibaru (AS10042)		Kurumibaru (AS10042)		Noga (TK6155)		Kurumibaru (AS10042)		Hata (0923_12)		Noga (TK6155)		Hata (0923_12)		Hata (0923_12)		Hata (0923_12)		Noga (TK6155)		Hata (0923_12)		Hata (0923_12)		Katayama (TK11033)	
(wt.%)	Avg.	1σ	Avg.	1σ	Avg.	1σ	Avg.	1σ	Avg.	1σ	Avg.	1σ	Avg.	1σ	Avg.	1σ	Avg.	1σ	Avg.	1σ	Avg.	1σ	Avg.	1σ	Avg.	1σ	Avg.	1σ	Avg.	1σ
SiO_2	67.04	0.03	72.38	0.44	72.40	0.38	71.84	0.37	72.61	0.28	73.27	0.28	69.57	0.30	71.00	0.31	70.48	0.24	70.74	0.41	71.03	0.39	71.20	0.20	73.13	0.38	70.39	0.16	68.38	0.22
TiO_2	0.61	0.02	0.37	0.08	0.36	0.03	0.36	0.02	0.35	0.03	0.33	0.03	0.61	0.03	0.60	0.02	0.60	0.01	0.61	0.01	0.60	0.01	0.46	0.04	0.34	0.02	0.57	0.03	0.70	0.04
Al_2O_3	16.52	0.66	15.05	0.35	14.96	0.24	14.96	0.16	14.84	0.15	14.62	0.13	15.60	0.19	15.01	0.13	15.09	0.24	14.95	0.28	14.89	0.15	15.28	0.10	14.54	0.26	15.24	0.12	15.58	0.16
FeO	3.26	0.38	1.40	0.12	1.38	0.09	1.48	0.12	1.31	0.07	1.26	0.07	2.35	0.09	2.07	0.07	2.11	0.06	2.06	0.10	2.08	0.13	1.71	0.09	1.28	0.08	2.17	0.04	2.84	0.15
MnO	0.15	0.02	0.09	0.02	0.09	0.02	0.10	0.01	0.09	0.02	0.08	0.02	0.11	0.02	0.09	0.02	0.10	0.01	0.10	0.01	0.10	0.01	0.09	0.02	0.09	0.02	0.09	0.02	0.12	0.02
MgO	0.93	0.14	0.29	0.03	0.31	0.05	0.33	0.03	0.26	0.04	0.24	0.03	0.70	0.03	0.49	0.03	0.55	0.02	0.53	0.07	0.51	0.02	0.40	0.03	0.24	0.04	0.55	0.02	0.83	0.03
CaO	2.81	0.23	1.00	0.06	1.01	0.08	1.06	0.11	0.94	0.05	0.86	0.06	1.98	0.07	1.43	0.04	1.51	0.10	1.43	0.11	1.33	0.06	1.30	0.07	0.88	0.08	1.64	0.04	2.25	0.09
Na_2O	4.63	0.08	4.40	0.15	4.43	0.11	4.67	0.12	4.33	0.19	4.23	0.13	4.46	0.08	4.31	0.36	4.57	0.10	4.54	0.20	4.35	0.21	4.31	0.14	4.00	0.22	4.34	0.07	4.41	0.09
K_2O	3.82	0.31	4.87	0.10	4.91	0.13	5.04	0.13	5.13	0.14	4.97	0.12	4.43	0.05	4.83	0.08	4.77	0.11	4.85	0.24	4.92	0.12	5.07	0.15	5.36	0.14	4.80	0.10	4.63	0.11
P_2O_5	0.14	0.03	0.03	0.02	0.04	0.03	0.05	0.01	0.04	0.02	0.03	0.02	0.09	0.03	0.07	0.03	0.09	0.01	0.09	0.01	0.09	0.01	0.06	0.02	0.03	0.01	0.11	0.03	0.18	0.03
Cl	0.09	0.02	0.10	0.02	0.11	0.02	0.11	0.01	0.10	0.01	0.10	0.02	0.11	0.01	0.09	0.01	0.10	0.01	0.09	0.01	0.10	0.02	0.11	0.01	0.11	0.02	0.10	0.02	0.10	0.02
(n)	*2*		*22*		*22*		*11*		*17*		*15*		*12*		*24*		*16*		*14*		*16*		*21*		*27*		*8*		*16*	
(ppm)	Avg.	1σ	Avg.	1σ	Avg.	1σ	Avg.	1σ	Avg.	1σ	Avg.	1σ	Avg.	1σ	Avg.	1σ	Avg.	1σ	Avg.	1σ	Avg.	1σ	Avg.	1σ	Avg.	1σ	Avg.	1σ	Avg.	1σ
V			13.1	1.1	12.9	0.9	12.9	0.8	12.2	0.9	13.3	0.5			32.6	1.4	33.5	1.1	31.3	0.4	32.3	2.1	17.0	5.8	13.7	2.0	28.2	0.9	38.5	1.1
Rb	-	-	166	6	167	4	169	10	171	5	181	2	-	-	170	5	176	7	176	4	172	4	198	26	191	5	172	4	163	3
Sr	-	-	160	20	146	18	147	10	136	16	120	4	-	-	191	7	196	8	176	11	185	17	196	26	109	16	214	5	288	4
Y	-	-	33.3	1.0	33.8	1.0	34.7	1.9	33.4	2.0	32.7	1.0	-	-	35.5	1.0	34.1	1.2	33.7	0.8	36.4	3.4	33.0	1.3	32.4	1.0	32.5	1.5	31.5	0.5
Zr	-	-	301	8	302	11	307	26	294	17	299	9	-	-	298	9	282	17	288	6	298	9	333	32	293	5	290	13	271	5
Nb	-	-	16.2	0.8	16.1	0.4	16.0	0.9	15.8	0.9	16.3	0.2	-	-	16.8	0.5	16.0	0.5	16.2	0.2	16.7	0.6	18.0	1.9	16.7	0.3	16.5	0.3	16.0	0.2
Ba	-	-	806	24	808	16	809	45	762	46	769	16	-	-	874	28	825	32	829	19	843	17	869	37	748	15	811	13	797	22
La	-	-	33.6	1.1	34.4	1.1	35.0	1.6	33.9	2.3	34.1	0.8	-	-	35.1	1.3	33.0	2.5	33.3	0.9	34.8	0.7	37.3	2.3	35.0	1.0	33.8	1.4	33.1	0.6
Ce	-	-	72.6	3.6	73.8	2.4	73.0	3.0	73.4	5.2	73.8	1.7	-	-	75.5	3.5	74.2	2.6	73.9	2.1	76.9	1.4	79.8	4.7	75.7	1.8	74.5	3.3	72.0	1.0
Pr	-	-	8.65	0.3	8.56	0.3	8.74	0.6	8.50	0.4	8.5	0.3	-	-	8.94	0.4	8.6	0.4	8.4	0.2	9.0	0.4	9.06	0.5	8.6	0.4	8.39	0.2	8.33	0.1
Nd	-	-	35.2	0.9	35.1	1.3	35.9	1.9	33.7	2.9	33.7	0.9	-	-	36.8	1.3	35.0	1.9	35.0	1.2	36.8	2.3	35.8	1.9	34.6	1.4	35.5	0.8	34.3	1.2
Sm	-	-	7.00	0.4	7.10	0.5	7.47	0.5	7.08	0.8	6.9	0.3	-	-	8.02	0.4	7.6	0.4	7.5	0.2	8.0	0.8	7.45	0.6	7.0	0.4	7.6	0.6	7.3	0.4
Eu	-	-	1.31	0.1	1.31	0.1	1.38	0.1	1.21	0.1	1.2	0.0	-	-	1.47	0.1	1.4	0.1	1.4	0.0	1.5	0.1	1.33	0.1	1.1	0.1	1.3	0.0	1.5	0.1
Gd	-	-	5.87	0.3	6.18	0.5	6.11	0.3	5.90	0.5	5.5	0.3	-	-	6.37	0.3	6.1	0.5	6.0	0.2	6.7	0.6	6.07	0.5	5.8	0.4	6.0	0.5	5.8	0.3
Dy	-	-	5.81	0.4	5.93	0.4	5.86	0.4	5.78	0.5	5.7	0.2	-	-	6.32	0.3	5.9	0.4	5.9	0.3	6.3	0.4	5.85	0.3	5.5	0.2	5.8	0.2	5.5	0.2
Er	-	-	3.56	0.2	3.61	0.2	3.69	0.2	3.64	0.2	3.6	0.1	-	-	4.00	0.3	3.6	0.3	3.6	0.1	3.9	0.4	3.67	0.3	3.5	0.2	3.5	0.2	3.5	0.1
Yb	-	-	3.82	0.2	4.11	0.3	4.00	0.3	3.81	0.3	3.9	0.2	-	-	4.02	0.2	3.8	0.2	3.8	0.1	4.2	0.5	3.82	0.3	3.7	0.2	3.7	0.3	3.4	0.1
Lu	-	-	0.58	0.05	0.61	0.02	0.59	0.05	0.61	0.06	0.59	0.02	-	-	0.60	0.04	0.58	0.04	0.57	0.02	0.63	0.06	0.58	0.03	0.57	0.04	0.54	0.05	0.54	0.02
Hf	-	-	7.67	0.5	7.88	0.4	8.08	0.7	7.83	0.5	8.2	0.3	-	-	7.97	0.3	7.4	0.7	7.6	0.3	7.8	0.2	8.89	1.0	8.0	0.3	7.44	0.7	7.31	0.3
Ta	-	-	1.17	0.0	1.19	0.0	1.20	0.1	1.13	0.1	1.2	0.0	-	-	1.21	0.0	1.1	0.1	1.2	0.0	1.2	0.0	1.33	0.2	1.3	0.0	1.17	0.1	1.11	0.0
Pb	-	-	23.9	1.0	23.7	1.0	23.2	0.8	23.2	1.4	24.6	0.4	-	-	23.7	0.9	23.3	1.4	23.6	0.6	24.2	1.6	25.9	2.2	25.5	1.6	23.3	0.6	21.8	0.4
Th	-	-	16.1	0.8	16.6	0.6	16.4	1.2	16.1	1.4	17.0	0.6	-	-	16.7	0.9	15.1	1.1	15.3	0.7	15.8	0.4	19.2	3.0	18.0	0.6	15.7	1.2	14.4	0.6
U	-	-	4.79	0.1	4.84	0.2	4.79	0.4	4.85	0.4	5.1	0.2	-	-	4.85	0.2	4.6	0.3	4.7	0.2	4.9	0.2	5.56	0.9	5.3	0.2	4.72	0.2	4.44	0.2
(n)	*-*		*9*		*12*		*10*		*9*		*11*		*-*		*12*		*10*		*11*		*9*		*12*		*7*		*4*		*7*	

(*continued on next page*)

Table 2 (*continued*)

Tephra	Aso-H (middle)		Aso-H (upper)		Aso-H (top)		Aso-I (base)		Aso-I (top)		Aso-J (base)		Aso-J (middle)		Aso-K (lower)		Aso-K (upper)		Aso-L		Aso-L		Aso-M		Aso-N/Z2 (lower)		Aso-N/Z2 (upper)		Aso-Z6	
Material	Pumice		Pumice		Ash		Pumice		Pumice		Pumice		Pumice		Pumice		Pumice		Pumice		Pumice		Pumice		Pumice		Ash		Pumice	
Sample id	FLF213		FLF217		FLF219		FLF206		FLF207		FLF202		FLF203		FLF200		FLF201		FLF197		FLF247		FLF72		FLF67		FLF69		FLF227	
Location	Katayama (TK11033)		Katayama (TK11033)		Katayama (TK11033)		Katayama (TK11033)		Katayama (TK11033)		Katayama (TK11033)		Katayama (TK11033)		Katayama (TK11033)		Katayama (TK11033)		Katayama (TK11033)		Noga (TK6155)		Noga (TK6155)		Noga (TK6155)		Noga (TK6155)		Katayama (TK11033)	
(wt.%)	Avg.	1σ	Avg.	1σ	Avg.	1σ	Avg.	1σ	Avg.	1σ	Avg.	1σ	Avg.	1σ	Avg.	1σ	Avg.	1σ	Avg.	1σ	Avg.	1σ	Avg.	1σ	Avg.	1σ	Avg.	1σ	Avg.	1σ
SiO_2	69.07	0.25	69.14	0.17	69.32	0.20	69.51	0.29	69.73	0.56	68.37	0.18	68.69	0.13	68.42	0.19	68.44	0.14	69.52	0.20	69.51	0.17	67.88	0.55	72.91	0.13	73.00	0.12	67.12	0.38
TiO_2	0.67	0.03	0.67	0.03	0.67	0.03	0.65	0.04	0.63	0.06	0.72	0.03	0.72	0.05	0.72	0.03	0.72	0.03	0.66	0.03	0.66	0.03	0.72	0.04	0.28	0.02	0.25	0.02	0.63	0.05
Al_2O_3	15.43	0.07	15.36	0.12	15.31	0.14	15.40	0.15	15.36	0.13	15.55	0.11	15.48	0.10	15.58	0.10	15.55	0.09	15.42	0.13	15.49	0.16	15.82	0.24	14.14	0.09	14.11	0.10	15.96	0.49
FeO	2.63	0.13	2.65	0.07	2.61	0.07	2.43	0.11	2.37	0.21	2.89	0.08	2.84	0.08	2.89	0.07	2.88	0.07	2.49	0.09	2.47	0.08	3.03	0.21	1.84	0.08	1.80	0.05	3.47	0.33
MnO	0.10	0.03	0.11	0.02	0.11	0.02	0.10	0.02	0.10	0.02	0.11	0.02	0.11	0.02	0.12	0.02	0.12	0.02	0.09	0.03	0.09	0.03	0.11	0.03	0.05	0.02	0.06	0.01	0.10	0.02
MgO	0.71	0.05	0.71	0.03	0.70	0.05	0.65	0.04	0.62	0.09	0.81	0.03	0.76	0.03	0.79	0.03	0.80	0.04	0.63	0.03	0.63	0.04	0.84	0.07	0.15	0.02	0.14	0.03	0.88	0.20
CaO	1.97	0.07	1.95	0.07	1.86	0.07	1.86	0.09	1.77	0.21	2.21	0.04	2.11	0.10	2.24	0.08	2.21	0.05	1.81	0.02	1.80	0.03	2.24	0.18	0.82	0.02	0.83	0.02	2.65	0.24
Na_2O	4.36	0.11	4.27	0.11	4.26	0.14	4.34	0.10	4.29	0.08	4.34	0.11	4.21	0.12	4.32	0.13	4.30	0.08	4.19	0.11	4.21	0.16	4.42	0.19	3.41	0.08	3.37	0.16	3.99	0.14
K_2O	4.81	0.08	4.87	0.10	4.91	0.12	4.82	0.09	4.88	0.15	4.74	0.07	4.81	0.09	4.67	0.10	4.70	0.09	4.98	0.11	4.94	0.13	4.70	0.18	6.26	0.10	6.27	0.21	4.91	0.23
P_2O_5	0.16	0.04	0.17	0.05	0.16	0.03	0.12	0.04	0.14	0.05	0.18	0.03	0.18	0.03	0.16	0.04	0.18	0.03	0.14	0.03	0.13	0.03	0.16	0.07	0.02	0.01	0.03	0.02	0.19	0.02
Cl	0.10	0.01	0.09	0.01	0.09	0.01	0.10	0.02	0.10	0.02	0.10	0.01	0.08	0.02	0.09	0.01	0.09	0.01	0.08	0.01	0.08	0.01	0.10	0.05	0.13	0.01	0.13	0.01	0.09	0.02
(n)	*18*		*18*		*19*		*20*		*18*		*19*		*17*		*18*		*18*		*19*		*10*		*12*		*12*		*14*		*13*	
(ppm)	Avg.	1σ	Avg.	1σ	Avg.	1σ	Avg.	1σ	Avg.	1σ	Avg.	1σ	Avg.	1σ	Avg.	1σ	Avg.	1σ	Avg.	1σ	Avg.	1σ	Avg.	1σ	Avg.	1σ	Avg.	1σ	Avg.	1σ
V	32.8	2.5	34.1	1.3	34.6	1.6	30.7	1.7	30.9	2.6	32.6	0.5					33.4	0.6			24.9	0.7							41.4	2.9
Rb	166	4	168	2	170	5	182	3	181	4	178	7	-	-	-	-	169	3	-	-	181	2	-	-	-	-	-	-	190	5
Sr	241	22	244	8	244	7	244	14	248	17	287	13	-	-	-	-	294	6	-	-	247	2	-	-	-	-	-	-	345	27
Y	31.1	0.8	32.5	0.5	33.3	0.4	33.0	1.2	33.9	2.1	32.4	0.8	-	-	-	-	33.3	0.6	-	-	33.4	0.5	-	-	-	-	-	-	29.9	2.4
Zr	276	8	292	3	300	3	292	11	301	17	278	8	-	-	-	-	287	5	-	-	303	5	-	-	-	-	-	-	290	21
Nb	16.2	0.5	16.6	0.1	17.1	0.2	17.2	0.4	17.5	0.9	16.5	0.3	-	-	-	-	16.9	0.3	-	-	17.5	0.2	-	-	-	-	-	-	16.6	0.9
Ba	786	21	807	15	819	16	827	25	841	27	805	27	-	-	-	-	821	11	-	-	845	13	-	-	-	-	-	-	767	49
La	32.8	1.2	34.3	0.4	35.4	0.4	34.8	1.2	36.0	2.3	33.8	1.2	-	-	-	-	35.0	0.7	-	-	35.7	0.4	-	-	-	-	-	-	34.2	2.6
Ce	71.9	1.9	74.5	1.0	77.1	1.2	75.1	3.1	76.4	5.6	74.5	2.6	-	-	-	-	76.3	1.6	-	-	77.7	1.0	-	-	-	-	-	-	74.7	4.3
Pr	8.27	0.2	8.61	0.2	8.84	0.2	8.50	0.4	9.04	0.9	8.60	0.4	-	-	-	-	8.8	0.2	-	-	9.0	0.1	-	-	-	-	-	-	8.5	0.5
Nd	34.1	0.9	36.1	0.5	37.0	0.8	35.4	1.7	37.1	3.6	35.5	2.0	-	-	-	-	37.1	0.8	-	-	36.6	0.8	-	-	-	-	-	-	35	3
Sm	7.1	0.3	7.6	0.5	7.6	0.2	7.5	0.6	7.5	1.1	7.8	0.4	-	-	-	-	7.69	0.35	-	-	7.73	0.23	-	-	-	-	-	-	7.08	0.74
Eu	1.4	0.1	1.4	0.1	1.5	0.1	1.5	0.1	1.6	0.1	1.6	0.1	-	-	-	-	1.61	0.09	-	-	1.47	0.19	-	-	-	-	-	-	1.39	0.10
Gd	5.7	0.3	6.2	0.3	6.6	0.3	6.3	0.5	6.4	0.7	6.3	0.3	-	-	-	-	6.30	0.19	-	-	6.32	0.29	-	-	-	-	-	-	5.68	0.54
Dy	5.5	0.3	5.8	0.4	6.2	0.2	5.7	0.4	5.9	0.5	5.7	0.3	-	-	-	-	5.97	0.34	-	-	5.93	0.17	-	-	-	-	-	-	5.25	0.36
Er	3.4	0.2	3.6	0.2	3.7	0.2	3.5	0.2	3.7	0.4	3.5	0.2	-	-	-	-	3.57	0.19	-	-	3.57	0.14	-	-	-	-	-	-	3.13	0.31
Yb	3.5	0.2	3.7	0.2	3.9	0.2	3.9	0.1	3.9	0.3	3.5	0.3	-	-	-	-	3.65	0.28	-	-	3.82	0.18	-	-	-	-	-	-	3.24	0.21
Lu	0.52	0.04	0.55	0.03	0.57	0.02	0.55	0.04	0.57	0.06	0.52	0.06	-	-	-	-	0.55	0.03	-	-	0.56	0.02	-	-	-	-	-	-	0.48	0.04
Hf	7.38	0.4	7.83	0.3	7.97	0.3	7.62	0.4	7.83	0.3	7.33	0.4	-	-	-	-	7.6	0.3	-	-	7.9	0.1	-	-	-	-	-	-	7.7	0.8
Ta	1.13	0.1	1.20	0.0	1.23	0.0	1.20	0.1	1.19	0.1	1.17	0.1	-	-	-	-	1.2	0.0	-	-	1.3	0.0	-	-	-	-	-	-	1.2	0.1
Pb	23.0	1.1	23.0	0.6	23.4	0.8	24.0	1.1	24.0	1.3	23.3	1.1	-	-	-	-	24.0	0.6	-	-	24.6	0.7	-	-	-	-	-	-	23.2	1.5
Th	15.0	0.6	15.8	0.4	16.3	0.4	15.7	1.1	15.9	1.1	14.9	1.2	-	-	-	-	15.8	0.4	-	-	16.6	0.3	-	-	-	-	-	-	17.0	1.6
U	4.78	0.7	4.72	0.1	4.78	0.1	4.60	0.3	4.64	0.4	4.42	0.3	-	-	-	-	4.6	0.1	-	-	4.9	0.1	-	-	-	-	-	-	5.0	0.4
(n)	*11*		*8*		*7*		*15*		*9*		*10*		-		-		*10*		-		*12*		-		-		-		*8*	

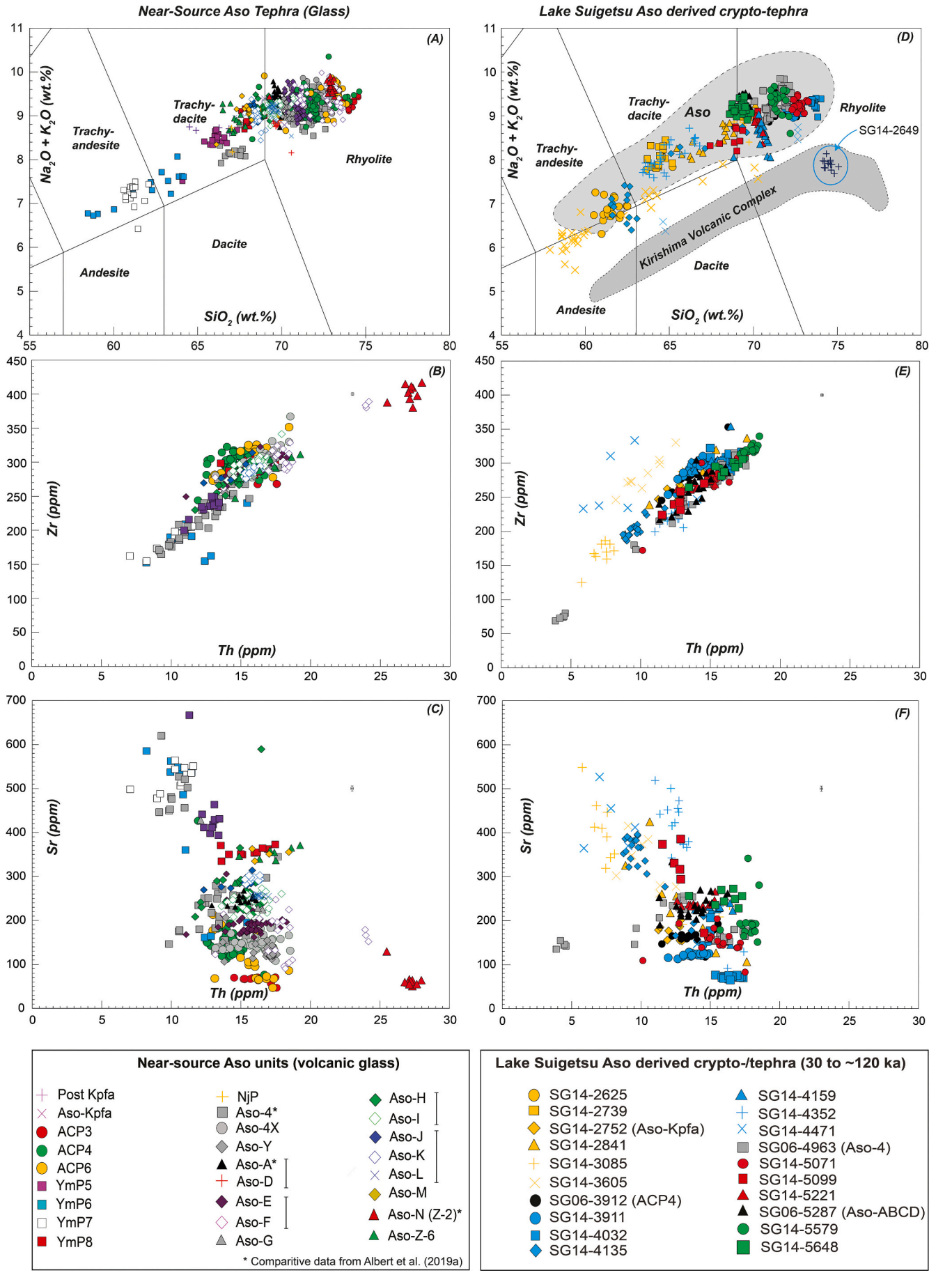

(caption on next page)

Fig. 4. (A-C) Major (WDS-EMP) and trace element (LA-ICP-MS) glass compositions of the Aso tephra units preserved in proximal outcrops around the Aso caldera between the Aso-3 (~130 ka) and AT (~30 ka) marker beds. Compositional fields Aso and Kirishima are from proximal data presented in previous studies for Aso from Smith et al., 2013 (Aso-A, Aso-D, Aso-4), Albert et al., 2019a (Aso = ACP3, ACP4, ACP5, ACP6, Aso-4, Aso-Y, Aso-A, Aso-B, Aso-C, Aso-D, Aso-I, Aso-K, Aso-M, Aso-N [Z2], Aso-3); and McLean et al., 2020 (Aso = Aso-Kpfa). Kirishima data are from Albert et al., 2024 (Kr-Kb) and Vineberg et al., 2024. (Kr-Aw, Kr-Iw). (D-F) Major and trace element glass compositions of the Aso crypto-/tephra deposits preserved in the Lake Suigetsu (SG14) sediments spanning 120–30 ka reported in: Vineberg et al. (2024), McLean et al. (2020), Albert et al. (2019a) and Smith et al. (2013). SG14–2649 was previously attributed to Aso activity (see McLean et al., 2020), but based on the similarity with glass compositions of Kirishima eruptions (Vineberg et al., 2024) this Suigetsu layer must be associated with an eruption of Kirishima. Veritcle lines in the key denote the sub-units of the same eruption.

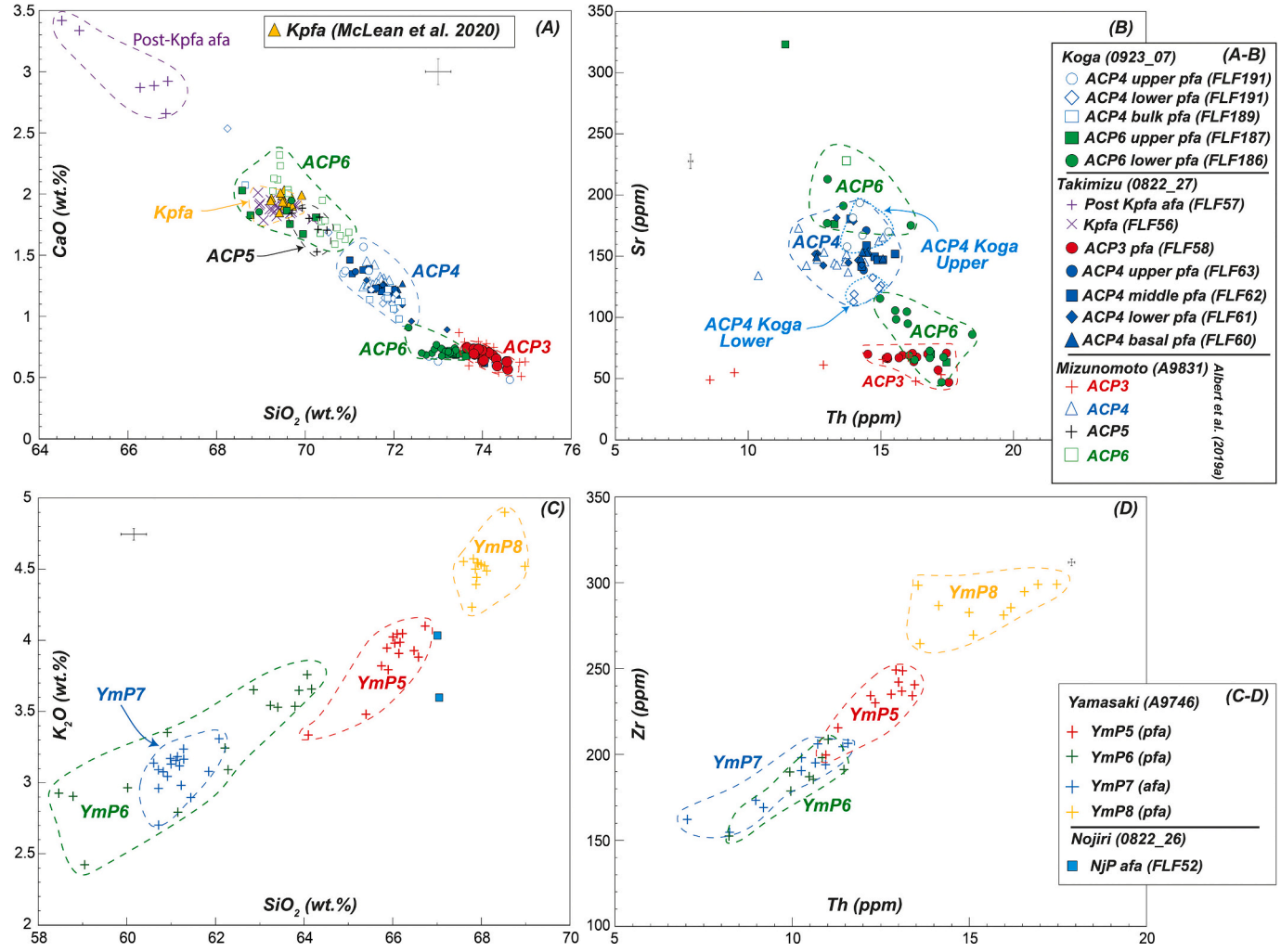

Fig. 5. Major (WDS-EMP) and trace element (LA-ICP-MS) geochemical variability of volcanic glasses from large magnitude silicic eruptions between the Aso-4 and AT tephra layers preserved in outcrops to the east of the caldera wall (locations shown in Fig. 1) in comparison with other proximal deposits previously analysed (McLean et al., 2020; Albert et al., 2019a). Error bars represent 2× standard deviation of repeat analyses of the StHs6/80-G MPI-DING standard glass.

more silicic YmP5 (SiO_2 = 66.0 ± 0.6 wt%; $Na_2O + K_2O$ = 8.4 ± 0.3 wt % [*n = 14*]) and YmP8 (SiO_2 = 68.0 ± 0.4 wt%; $Na_2O + K_2O$ = 8.9 ± 0.1 wt% [*n = 13*]) trachy-dacite pumice deposits are more easily distinguished (Fig. 5), while the trachy-andesite to trachy-dacite YmP6 and YmP7 units are compositionally similar to one another, albeit the younger YmP6 deposits spans a broader compositional range (Table 2; Fig. 5). Similarly, these deposits can be distinguished from each other at the trace element level, consistent with major element composition, YmP8 pumices are more enriched in incompatible trace elements (e.g., 286 ± 12 ppm Zr; 15.5 ± 1.4 ppm Th) than the YmP5 pumices (e.g. 233 ± 14 ppm Zr; 12.6 ± 0.8 ppm Th; Fig. 5D). The YmP6 and YmP7 volcanic glasses are less enriched in incompatible trace elements, and again show similar compositions (Fig. 4; 5D).

The NjP dispersed to the SE of the caldera is the first thick tephra unit erupted post-Aso-4 (Miyabuchi et al., 2003) and occurs below the YmP series. The NjP were highly weathered, which hindered our ability to obtain detailed geochemical data for this tephra. Only two major element analyses were acquired for the NjP, which were from the ash layer separating the two pumice units. These glasses are trachy-dacitic (SiO_2 = 67 wt%; $Na_2O + K_2O$ = 8.2–8.7 wt%) and show a similar degree of evolution to the stratigraphically younger YmP5 glasses (Fig. 5C-D).

4.2. Aso-4 and Aso-4X

The Aso-4 PDC has three geochemically distinct components at the major and trace element level, and the two rhyolitic components are widely dispersed from the volcano (Fig. 6 A-B; Albert et al., 2019a). Samples were also taken stratigraphically through the Aso-4X fall unit at Kurumibaru, and these represent the first glass geochemical data for this

unit. The Aso-4X glasses are homogeneous rhyolites with 72.3 ± 0.5 wt % SiO_2, 1.4 ± 0.1 wt% FeOt, and 1.0 ± 0.08 wt% CaO (1σ; *n = 55)*. The trace element compositions of the Aso-4X are also homogeneous (Zr = 302 ± 17 ppm; Th = 16.3 ± 1.1 ppm; Sr 148 ± 15 ppm [1σ]), displaying no geochemical differences stratigraphically throughout the fall unit (Fig. 6A-B; Table 2). The major and trace element glass compositions of the Aso-4X fall deposit broadly overlap with the most evolved, glass Component 1, of the Aso-4 PDC deposits (Albert et al., 2019a). However they do extend to higher levels of incompatible trace element enrichment (e.g. Th = 16.3 ± 1.1 ppm; Zr = 302 ± 17 ppm [1σ]) than those of the Aso-4 PDC (e.g., Component 1; 260 ± 20 ppm Zr; Fig. 4B), and are thus more consistent with the Aso-Y glasses that erupted during the older pre-Aso-4, Stage 5 (Fig. 6B).

4.3. Stage 5 (Aso-Y)

The Aso-Y unit is a pumice fall deposit, and the only tephra deposit reported in the paleaosol separating the Aso-4/Aso-4X and Aso-ABCD, and ultimately in the 10 kyr prior to the Aso-4 caldera-forming eruption (Table 1; Fig. 3; Hoshizumi et al., 2022). Aso-Y was sampled at Kurumibaru and re-sampled at 11 km ENE at Noga (Fig. 1D, 2). The glass data here from both Noga and Kurumibaru show a compositional overlap, with these rhyolitic (ca. 73 wt% SiO_2) glasses are indistinguishable, and overlap with previously published Aso-Y compositions, thus verifying the tephrostratigraphic correlation between Noga and Kurumibaru (Fig. 6A-B). The Aso-Y compositions also share overlapping major and trace element compositions with the overlying Aso-4X and Aso-4 PDC (component 1) (Fig. 6A-B).

4.4. Stage 4 (Aso-ABCD, Aso-EF, Aso-G, Aso-HI, Aso-JKL, Aso-M)

Here we outline the geochemical features of the tephra units (sub-units) that make up the six pre-Aso-4 Stage 4 eruptions. The Aso-ABCD tephra represents the largest eruption post Aso-3 and pre-Aso-4 (Stage 4; Table 1), and all its sub-units have previously been characterised from the outcrop at Noga (see Albert et al., 2019a). Here we provide additional major element data for the Aso-D unit sampled at Hata where it is dissected by the Aso-4 PDC. The homogeneous Aso-D rhyolitic glasses (SiO_2 = 69.7 ± 0.4 wt%; $Na_2O + K_2O$ = 8.8 ± 0.2 wt%; *n = 13*) from Hata are consistent with previously published data for this sub-unit, which extend to higher CaO (2.0 ± 0.1 wt%) contents than the pumices of Aso-ABC (> 2 wt%; Fig. 6C).

The Aso-EF eruption (Fig. 6C-D) was characterised using outcrops at Hata and Noga (Fig. 1D). The lowermost fall deposits of Aso-EF, the Aso-F pumice bed has a rhyolitic glass composition, with Aso-F glasses preserved at Hata (SiO_2 = 73.1 ± 0.4 wt%; CaO = 0.9 ± 0.1 wt% [1σ; *n = 27*]) being more evolved than those sampled at Noga (SiO_2 = 71.2 ± 0.2 wt%; CaO = 1.3 ± 0.1 wt% [1σ; *n = 21*]), and they are distinguishable based on SiO_2, CaO and FeOt contents (Table 2; Fig. 6C). The overlying Aso-E volcanic glasses are again homogeneous rhyolites (SiO_2 = 70.8 ± 0.4 wt%; $Na_2O + K_2O$ = 9.3 ± 0.3 wt% [1σ; *n = 70*]) with sub-unit samples indistinguishable from each other regardless of sampling locality or stratigraphic position (Fig. 6C). The glass compositions of these Aso-E deposits are less evolved than those of the initial Aso-F fall deposits of the eruption, whilst more evolved than the products of younger Aso-ABCD eruption. At a trace element level, the Aso-E glasses can clearly be distinguished from the overlying Aso-ABCD tephra owing to their lower Sr (191 ± 23 ppm [1σ; *n = 43*]) content at an overlapping Th content (Fig. 6D). The Aso-E and Aso-F (Noga) sub-units have overlapping levels of incompatible trace element enrichment, and similar Sr contents making discriminating them more difficult (Fig. 6D). Although the Noga Aso-F glasses (Zr = 333 ± 32 ppm; Th = 19.2 ± 3.0 ppm) are dominated by glasses with higher levels of incompatible trace element enrichment compared to those of the Aso-E (Zr =291 ± 13; Th = 15.7 ± 1.1 [1 σ; *n = 43*]; Fig. 6D).

Pumice lapilli associated with the Aso-G eruption were sampled from an outcrop located at Hata (Fig. 1D). The Aso-G rhyolitic glasses are homogeneous (SiO_2 = 70.3 ± 0.2 wt%; $Na_2O + K_2O$ = 9.2 wt% [1σ; *n = 18*]), with no stratigraphic chemical variability within the deposits (Fig. 6C–D), and these glasses overlap with other units erupted between Aso-3 and the AT tephras (Fig. 4 A-B). The Aso-HI eruptive succession related to the second largest Stage 4 eruption. Deposits associated with this eruption were sampled at Katayama (Fig. 1D).

Lower (FLF206) and Upper (FLF207) pumice samples of the Aso-I fall deposit reveal homogeneous rhyolites (SiO_2 = 69.6 ± 0.4; $Na_2O + K_2O$ = 9.2 ± 0.1 wt% [1σ; *n = 38*]) at Katayama with no chemo-stratigraphic variation at the major or trace element level (Fig. 6E-F). The Aso-I unit was previously sampled at an outcrop at Noga, 8 km northeast of Katayama (Albert et al., 2019a). The glasses from the Aso-I unit at Noga have higher CaO and FeOt content, and greater Sr (292 ± 16 ppm; 1σ) at a given Th content than the newly sampled Aso-I (Sr = 243 ± 17 ppm [1σ; *n = 29*]) glasses from Katayama, and thus they can be easily distinguished from each other using major and trace element compositions (Fig. 6E-F).

Owing to the thickness of the Aso-H unit, at Katayama, it was sampled for chemical at multiple stratigraphic levels (Fig. 3), chemical analyses were conducted on three pumice fall beds, one at the base (FLF208), one near the middle (FLF213), and in the upper portion (FLF217). A fourth sample related to a thick ash bed in the upper section of Aso-H. The homogenous basal rhyolitic pumices of Aso-H have lower SiO_2 (68.4 ± 0.2 wt%) and K_2O (4.6 ± 0.1 wt%), whilst higher CaO (2.2 ± 0.1 wt%; *n = 16*) content relative to the overlying other Aso-H units which cannot be distinguished from each other (SiO_2 = 69.2 ± 0.2; K_2O = 4.9 ± 0.1; CaO = 1.9 ± 0.1 wt% [1σ; *n = 55*]; Table 2). There is a large degree of trace element overlap between the basal Aso-H pumice bed and the overlying Aso-H samples (FLF213, FLF214; FLF217), however the lower most fall (FLF208) are dominated by glasses displaying higher Sr content (288 ± 4 ppm; *n = 7*) relative to those of the overlying Aso-H sub-units (Sr = 243 ± 15 ppm; *n = 26*; Fig. 6F). The chemical discrepancy between the Aso-I unit at Katayama and Noga raises questions marks over the stratigraphic correlation of Aso-I between the two sites. Interestingly, the basal Aso-H pumice fall at Katayama is compositionally identical to the Aso-I unit previously sampled from Noga (Fig. 6E-F). This might suggest that the opening eruptive phase of Aso-I is not recorded at Noga, and that this fall deposit, resting on a palaeosol, corresponds instead to the earliest phase of the Aso-H, as recorded at Katayama. Indeed, the earliest Aso-H fall deposit could serve as a chemo-stratigraphic marker within the Aso-HI eruptive succession. This is because the remaining upper Aso-H deposits (middle to upper) exhibit partial overlap in major element compositions, and complete overlap in trace element composition, with the underlying Aso-I unit at Katayama (Fig. 6E-F). Despite the thickness of the Aso-HI eruption, there is limited geochemical variation making correlations of specific sub-units challenging. The likely absence of Aso-I at Noga, and thinning between Katayama and Hinatame further north, might indicate that the plume of the climatic Plinian phase of Aso-I was predominantly dispersed towards the southeast and then migrated north.

Regarding the Aso-JKL eruption, these rhyolitic glasses display considerable compositional overlap with those of the Aso-HI eruption. Aso-K forms the thickest pumice beds at multiple localities (Fig. 3) and chemical analysis of the upper and lower portions at Katayama show no, observable compositional differences stratigraphically, as is the case for the Aso-J deposits (Fig. 6E). At Noga, located 10 km northeast of Katayama (Fig. 1D), only the Aso-L (5 cm thick) and Aso-K (20 cm thick) units are seen (Fig. 3; Hoshizumi et al., 2022). Aso-K rhyolites are chemically consistent between Katayama (SiO_2 = 68.4 ± 0.2; CaO = 2.2 ± 0.1; Sr = 294 ± 6 ppm) and those previously analysed from Noga (68.4 ± 0.4; CaO =2.2 ± 0.1 wt%; Sr =283 ± 20 ppm; Albert et al., 2019a). Similarly, the Aso-L units sampled at Katayama and Noga are chemically consistent (Fig. 6 E-F). The major element compositions of the youngest units Aso-J and Aso-K show considerable overlap with each other, whilst the basal (older) Aso-L sub-unit is easily distinguished

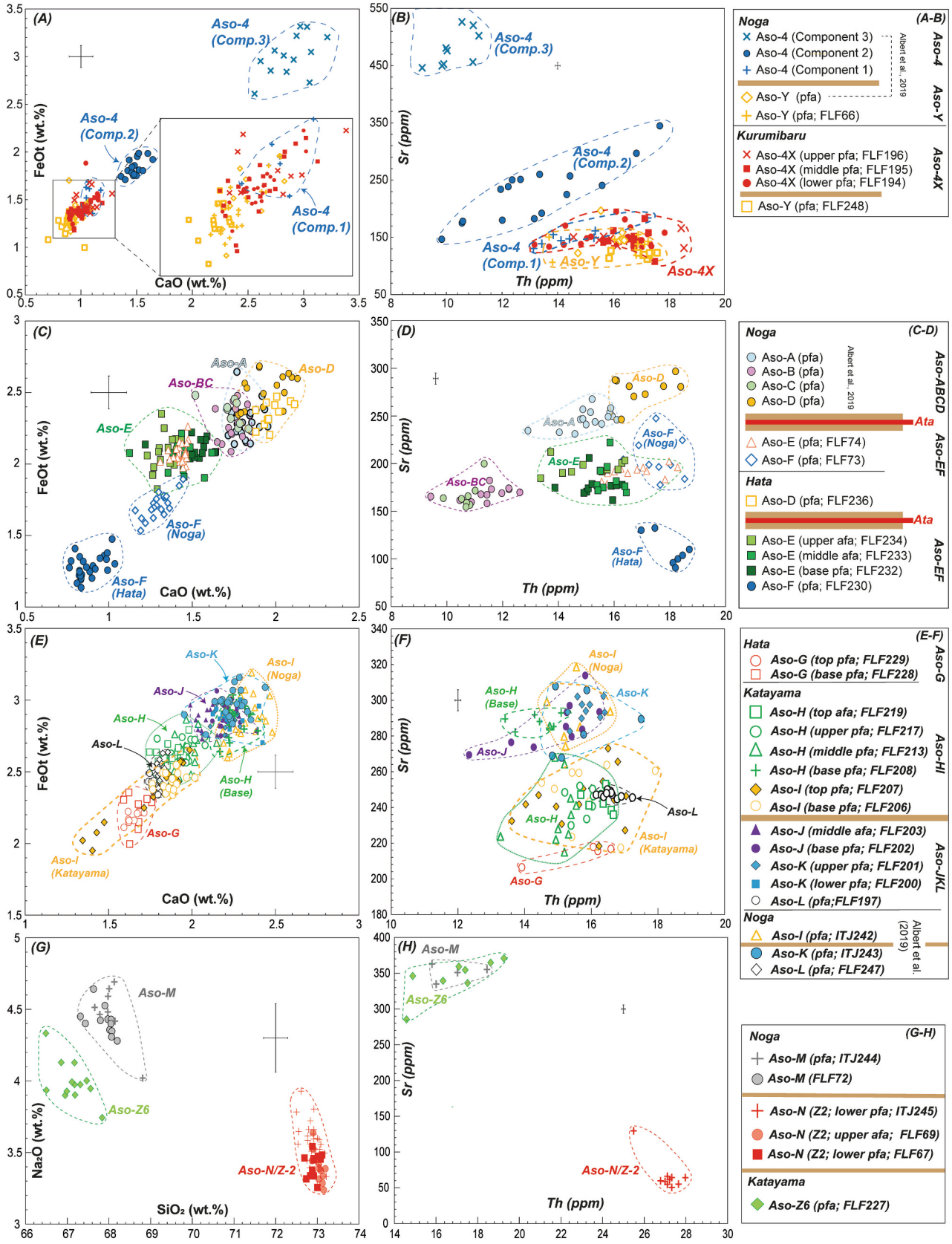

Fig. 6. Major (WDS-EMP) and trace element (LA-ICPMS) geochemical variability of volcanic glasses from large magnitude silicic eruptions that occurred between the Aso-3 and Aso-4 eruptions, preserved in outcrops to the east of the caldera wall (locations shown in Fig. 1 and units listed in Table 1). These compositions are shown in comparison with other proximal deposits previously analysed (Albert et al., 2019a). Error bars represent 2 x standard deviation of repeat analyses of the StHs6/80-G MPI-DING standard glass. Brown bars in the symbol legends denote palaeosols separating eruption units, in some case containing widespread tephra markers from other Japanese volcanic sources. (For interpretation of the references to colour in this figure legend, the reader is referred to the web version of this article.)

Table 3
Summary of the Aso derived crypto−/tephra layers identified in the sediments of the Lake Suigetsu (SG14 Core) between 130 and 30 ka. CD = Composite Depth position, V = visible, C = cryptotephra. The original manuscript reporting the tephra from Lake Suigetsu where it was first identified and labeled within the sedimentary sequence: a = McLean et al. (2020); b = Smith et al. (2013); c = Albert et al. (2019a); d = Vineberg et al. (2024). Glass shard Morphologies; PU = Pumiceous, B=Blocky, C=Cuspate, F=Fluted, V=Vesicular, MV = Microvesicular, MI = Microlite inclusions.

Tephra (SG14 label)	V = thickness (cm)/ c = shards/g		Glass shard morphology	Position in SG14 master core (cm)	SG14 CD (cm; ver. 28 Feb 2019)	SG06 CD (cm; ver. 28 Feb 2019)	IntCal20 Ka BP (median ± 1 s) or interpolated Ka	Major Element Glass Compositions (wt%)				Trace Element Analyses	Aso Tephra / Widespread marker
								SiO_2	K_2O	CaO	n	n	
SG06-2650[b,c]	**V**	**35.0**	**C**	**G-06 Bottom**	**2614.9**	**2615.2**	**30.2 ± 0.05**						**AT (Aira)**
SG14–2625[a]	C	9838	MI, C, V	E-23 (6.0–7.0)	2624.7	2637.9	30.3 ± 0.05	60.51–65.12	2.61–3.88	3.57–5.48	21	–	–
SG14–2739[a]	C	8367	PL, MI	F-28 (62.8–63.8)	2738.9	2763.8	32.5 ± 0.05	63.70–65.18	3.58–3.92	3.39–4.20	16	–	–
SG14–2752[a]	C	10,067	F, C, MV	F-28 (75.8–76.8)	2751.9	2776.3	32.7 ± 0.06	68.84–70.11	3.95–4.50	1.66–2.02	17	9	Aso-Kpfa
SG14–2841[a]	C	2850	PL, MI	E-30 (25.0–26.0)	2840.1	2861.4	35.0 ± 0.05	61.23–70.12	2.97–5.73	1.74–5.13	28	8	–
SG14–3085[a]	C	4400	PU	G-08 (52.0–53.0)	3084	3095.2	39.2 ± 0.06	57.89–68.16	1.88–4.55	2.56–6.95	28	12	–
SG14–3605[a]	C	2200	MI	E-37 (58.3–59.3)	3604.1	3629.3	45.5 ± 0.1	62.27–70.28	2.62–4.47	0.38–5.53	11	10	–
SG06–3912[b,c]	V	0.1	F	F-39 (61.0–61.1)	3878.9	3911.6	48.7 ± 0.2	69.64–73.63	4.46–4.90	1.05–2.33	20	16	ACP4 (Upper)
SG14–3911[d]	C	24,890	F, MV	E-40 (44.5–45.5)	3911.1	3941.9	49.1 ± 0.2	71.90–72.48	4.52–4.83	1.02–1.15	27	23	ACP4 (Lower)
SG14–4032[d]	C	8325	C, F	F-41 (9.0–10.0)	4031.7	4068.6	51.5 ± 1.0	72.13–74.03	4.60–5.03	0.66–1.02	19	17	ACP6
SG06–4141[b,c]	**V**	**1.3**	**C**	**E-42 (31.9–33.3)**	**4105.7**	**4141.2**	**54.3 ± 1.6**						**SAN1/Kj-P1/Hd (Kuju)**
SG14–4135[d]	C	>20,000	V	F-42 (30.9–31.9)	4135.4	4173.5	55.6 ± 1.8	61.54–69.60	2.74–4.44	1.98–5.65	20	20	–
SG14–4159[d]	C	19,510	B, C, MV	G-11 (22.4–23.4)	4158.7	4198.3	56.6 ± 1.9	68.83–71.02	3.34–4.58	1.65–2.57	19	9	–
SG14–4352[d]	C	5883	PU	F-44 (25.8–26.8)	4351.9	4388.6	64.1 ± 2.4	63.42–66.81	2.91–4.54	2.66–4.43	30	18	YmP5
SG14–4471[d]	C	1333	B, MV, MI	F-45 (41.9–42.9)	4470.6	4509.0	68.7 ± 2.5	64.63–73.51	3.23–4.53	1.01–4.39	10	7	–
SG06–4963[b, c]	**V**	**3.5**	**F, V**	**G-12 (57.2–60.7)**	**4922.8**	**4962.4**	**86.4 ± 0.6***	**70.06–72.38**	**4.04–4.83**	**0.97–1.67**	**62**	**46**	**Aso-4**
SG14–5071[d]	C	49,225	C, F	F-51 (25.8–26.8)	5071.5	5113.6	91.2 ± 1.8	72.31–73.27	4.55–4.89	0.82–1.06	19	18	Aso-4X?
SG14–5099[d]	C	67,850	MI, V	F-51 (53.4–54.4)	5098.5	5138.5	92.1 ± 2.0	67.42–70.26	3.14–4.43	1.51–3.22	9	–	–
SG06–5181[b,c]	**V**	**0.2**		**E-52 (55.3–55.5)**	**5142.2**	**5180.3**	**93.4 ± 2.2**						**K-Tz (Kikai)**
SG14–5221[d]	C	>20,000	C	F-52 (76.4–77.4)	5221	5257	96.0 ± 2.6	70.06–70.56	4.24–4.51	1.71–1.85	18	14	–
SG065287[b, c]	**V**	**3.5**	**MV**	**E-53 (52.5–56.0)**	**5250.6**	**5286.7**	**96.8 ± 2.7**	**69.19–69.88**	**4.43–4.65**	**1.69–1.92**	**18**	**21**	**Aso-ABCD**
SG14–5579[b, c]	V	0.8	C, MV	G-16 (19.1–20.1)	5578.8	5631.1	108.4 ± 4.0	71.03–72.20	4.89–5.20	1.09–1.37	22	17	Aso-EF
SG14–5648[d]	C	>20,000	MV	E-57 (46.2–47.2)	5648.3	5702.3	110.8 ± 4.2	69.85–68.59	4.50–5.01	1.70–2.26	40	8	Aso-HI

* Footnote * is derived from an $^{40}Ar/^{39}Ar$ age determination of the Aso-4 PDC rather than interpoltation (see methods). Those Lake Suigetsu tephra layers highlighted in bold relate to widespread Japanese tephra markers found in the tephrostratigraphy of Aso.

owing to lower CaO (1.8 ± 0.2 wt% *[n = 31]*), FeOt, and Sr (247 ± 2 ppm; *n = 12*) contents (Fig. 6E-F). While Aso-L glasses display a chemical overlap with those of older Aso-HI eruption deposits, they are far more homogeneous in their trace element signature (Fig. 6F), making the heterogeneity of the Aso-HI glasses a distinctive characteristic of this the second largest eruption of Stage 4. At the trace element level, the Aso-J and Aso-K glasses show a high degree of similarity, although the younger Aso-J glasses extend to lower Th contents (~12 ppm; Fig. 6F). The major element data obtained for Aso-M eruption deposit at Noga is consistent with previously published glass data, the Aso-M glasses are distinctive from the eruption units above (Aso-HI and Aso-JKL) owing to their higher Sr content (Fig. 4C).

4.5. Stage 3 (Aso-N [Z2] and Aso-Z6)

The lower pumice and upper ash fall of the Aso-N (Z2) tephra at Noga were geochemically analysed, and they cannot be distinguished from each other, they are consistent with previously published major element data from the lower pumice fall of this unit (Fig. 6G; Albert et al., 2019a). The Aso-Z6 tephra was sampled at Katayama (Fig. 3). The Aso-Z6 tephra is trachytic and is compositionally distinct from the younger Stage 3 tephra Aso-N (Z2) as it has lower SiO_2 (72.7–73.2 wt%) and higher CaO (0.8–0.9 wt%), appearing to be less evolved (Table 2; Fig. 6G-H). It is most consistent with chemical composition of the younger Aso-M eruption.

5. Discussion

5.1. Proximal-distal Aso correlations

Here we assess correlations between the proximal Aso tephra deposits and the pre-30 ka Aso derived tephra layers preserved in Lake Suigetsu using the new glass geochemical data obtained from the near-source areas, presented above. Although some tephra correlations have been previously made between Aso and Lake Suigetsu (McLean et al., 2020; Albert et al., 2019a; Smith et al., 2013), many layers have not yet been correlated to specific eruptions (Vineberg et al., 2024). Furthermore, while McLean et al. (2020) correlated the SG14–2649 cryptotephra to Aso, new glass data from Kirishima volcanic complex (Vineberg et al., 2024) suggests that SG14–2649 is more likely derived from Kirishima (Fig. 4D) and is therefore not discussed further in this study.

The twenty Aso tephra and cryptotephra deposits preserved in Lake Suigetsu beneath the AT tephra (Table 3) are found interspersed between many widespread tephra markers traced across the Japanese islands, and some of which also occur in the proximal volcanic stratigraphy of Aso. These therefore provide useful as chrono-stratigraphic markers to help correlate the deposits. The Lake Suigetsu Aso deposits range from trachy-andesites through trachy-dacites to rhyolites (Fig. 4D). Four of these have previously been assigned to specific eruptions based on geochemical links to proximal deposits: SG14–2752 with Aso-Kpfa; SG06–3912 with ACP4; SG06–4963 with Aso-4; and SG06–5287 with Aso-ABCD (see: McLean et al., 2020; Albert et al., 2019a; Smith et al., 2013). We focus on the six deposits beneath and thirteen tephra above the Aso-4 (SG06-4963) tephra in Lake Suigetsu, with the aim of linking them to proximal units to help improve understanding of the timing, frequency, and ash dispersals of past Aso eruptions.

5.2. Post-Aso-4

Of the thirteen Aso deposits preserved in the 23 m of sediment above the Aso-4 in Lake Suigetsu, five can now be firmly correlated to proximal counterparts (Table 3; This Study; Vineberg et al., 2024; McLean et al., 2020; Albert et al., 2019a). The SG14–2752 cryptotephra that is preserved 137 cm beneath the AT marker layer, was correlated by McLean et al. (2020) to the Aso-Kpfa, the largest and most voluminous pumice-fall deposit erupted from the post-Aso-4 cones (Fig. 7 AB; McLean et al., 2020). The cryptotephra deposits SG14–2739 and SG14–2625 are preserved in the 1.3 m of sediment above the Aso-Kpfa (SG14–2752) and below the AT, spanning a 2.5 kyr interval (Table 3). Both deposits also plot at the trachy-andesite/andesite boundary (Fig. 4), and are less evolved than the older Aso-Kpfa eruption unit. They can easily be distinguished from each other using major elements, becoming less evolved with time (Fig. 7A). The older SG14–2739 is preserved just 13 cm above the Aso-Kpfa (SG14–2752) cryptotephra, with a Lake Suigetsu age of 32.5 ± 0.05 ka. This cryptotephra shows a partial overlap with the least evolved glasses of the post Aso-Kpfa ash fall deposit at Takimizu (Fig. 7A). We therefore only tentatively correlate the SG14–2739 with this post Kpfa ash fall deposit. At Takimizu, there is no clear evidence of a temporal gap (palaeosol) between the units, and it could be possible to interpret this ash fall unit as part of the Kpfa eruption, however, the Lake Suigetsu record is clearly indicating that a pulse of activity occurs at Aso between ~32.7 and 30 kyrs, with widespread ash dispersal associated with more than simply just the main Plinian Aso-Kpfa eruption. Indeed, the sedimentation and cryptotephra deposits at Lake Suigetsu indicate far-travelled ash dispersals from Aso are separated by just 300 yrs. during this period of activity at the volcano. No prominent units in the investigated near-source Aso sequences were observed above the post Kpfa ash bed as candidates for the youngest pre-AT Aso cryptotephra (SG14–2625), but further near-source investigations of the deposits in this time interval could be useful to further constrain the repose intervals between eruptive events, and identify the deposits firmly associated with these cryptotephra deposits found above the Aso-Kpfa eruption deposit.

The three cryptotephra deposits - SG14–3605, SG14–3085 and SG14–2841 are deposited within the ~16 kyr of sediments between the previously reported ACP4 (SG06–3912) and Aso-Kpfa (SG14–2752) tephra layers at Lake Suigetsu (Table 3). The youngest, SG14–2841, can be distinguished from the older SG14–3085 and SG14–3605 deposits owing to higher SiO_2 and lower Sr content (Fig. 4D), whereas the underlying cryptotephra layers can be discriminated from each other using CaO vs. FeOt plots (Fig. 7C). Although these three deposits are in the same chrono-stratigraphic interval as the ACP3 tephra, for instance post ACP4 and prior to Aso-Kpfa, there are no compositional similarities (Fig. 7C). All three of the Lake Suigetsu cryptotephra layers have relatively low shard concentrations compared to other Aso tephra deposits at Lake Suigetsu (<5000 shards/g; Table 3), which could either infer a dominant tephra dispersal axis inconsistent with transport to Lake Suigetsu, or smaller magnitude eruptions at the volcano. While shard concentrations are not a direct proxy for eruption scale, owing to the influence of dominant wind patterns on tephra dispersal and ash fall concentrations, we do note that Aso cryptotephra shard concentrations at Lake Suigetsu typically reach 10,000 shards/**g,** and exceeding 50,000–60,000 shards/g, when associated with the larger known eruptions at the volcano (see Table 3). An association of these three cryptotephra to smaller explosive eruptions seems most plausible, given no thick, prominent, units are documented in near-source records east of the volcano, the only other chrono-stratigraphically relevant pumiceous candidate being the Mizunomoto Pumice 2 (Fig. 2; Miyabuchi, 2009). However, this tephra has a poorly defined distribution, and a very small volume estimate (Miyabuchi, 2009). With three cryptotephra preserved in this time-window at Lake Suigetsu, it would indicate the near-source candidates of these distal deposits are not well preserved in near-source area. Thus in addition to the ACP3 Plinian deposit, there must have been a further three eruptions in the 16 kyr interval, between the ACP4 activities and Aso-Kpfa eruption, capable of widespread ashfall events (Table 3).

The 1.0 mm thick visible tephra in Lake Suigetsu, SG06–3912 (SG14 CD 38.79 m) was attributed to the Plinian ACP4 eruption deposits (Albert et al., 2019a), and has an updated Lake Suigetsu age of 48.7 ± 0.19 ka (Table 3; Vineberg et al., 2024). Subsequently, Vineberg et al.

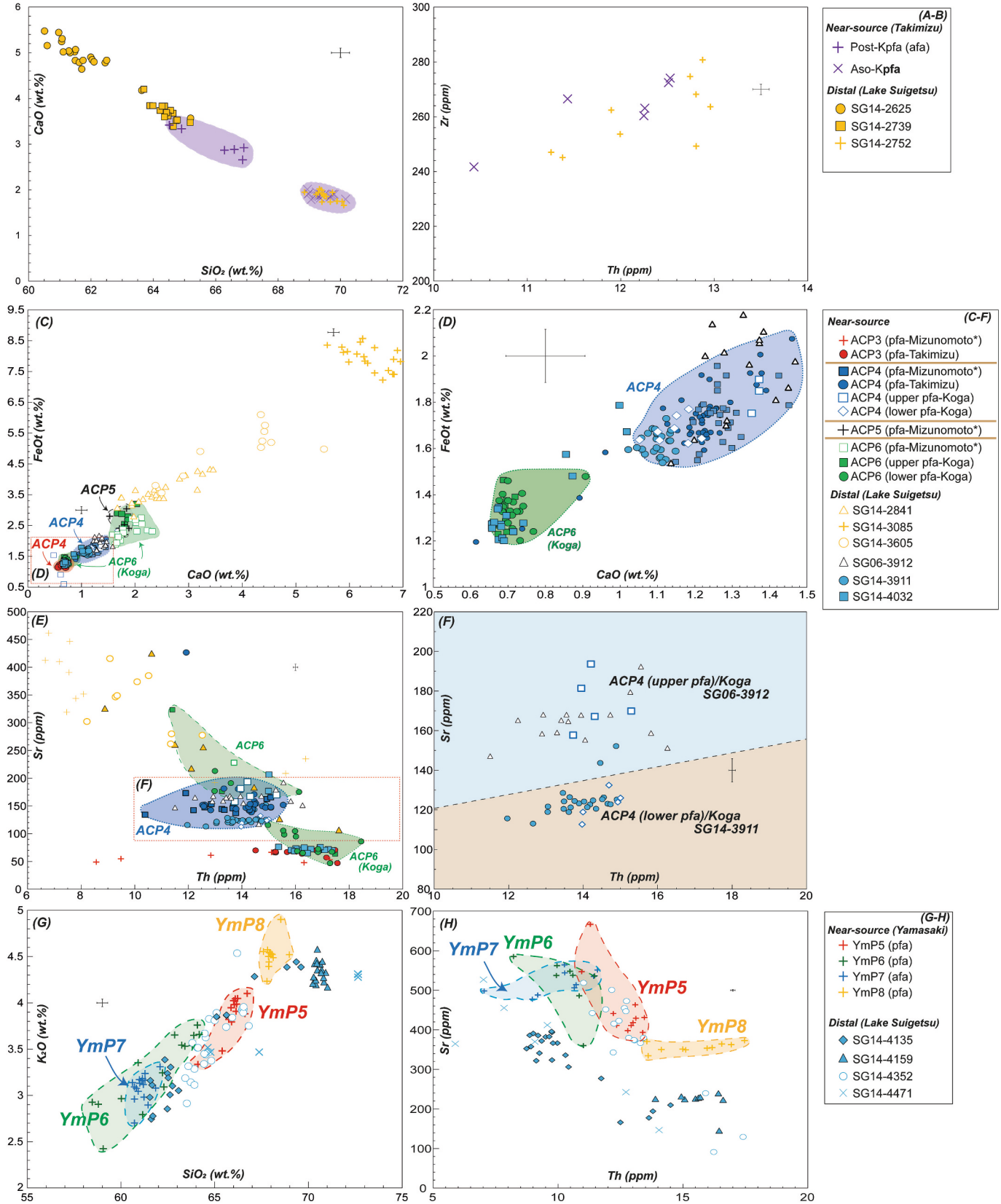

Fig. 7. Major and trace element glass compositions of the Aso crypto−/tephra deposits preserved between the Aso-4 and AT tephra layers in the Lake Suigetsu (SG14) sequence compared to reference chemical datasets produced for chrono-stratigraphically relevant eruption units. Reference chemical datasets obtained from proximal outcrops are from *This Study*, McLean et al. (2020), and Albert et al. (2019a). Error bars represent 2 x standard deviation of repeat analyses of the StHs6/80-G MPI-DING standard glass.

(2024) observed that a cryptotephra SG14–3911, 32 cm below SG06–3912, in the SG14 core, also shares a geochemical similarity with the ACP4 deposits, both in terms of major and trace element compositions (Fig. 7C-F). The two Lake Suigetsu tephra deposits, SG14–3911 and SG06–3912, separated by 32 cm of sediment, which represents a time interval of ~400 years. Importantly the tephra layers can be distinguished from each other both at a major and trace element level (Fig. 7C-F; Table 3). However, this is most convincingly observed in their Sr content, where the older cryptotephra, SG14–3911, displays greater depletion in Sr content relative to the younger SG06–3912 tephra (Fig. 7F). The acquisition of new trace element data from lower and upper units of the ACP4 tephra deposit preserved at Koga (NE of the caldera) are also distinguishable based on their Sr content (Fig. 7F). The older SG14–3911 cryptotephra glasses shows lower Sr content with a clear affinity with the Lower ACP4 deposits, whilst the younger SG06–3912 tephra shows an affinity with the ACP4 upper deposit at Koga, and the ACP4 deposit preserved to the East at Takimizu and Mizunomoto (Fig. 7C-E). Proximal and distal evidence confirms that the ACP4 tephra deposits record two temporally distinct eruptions separated by a 400 yr period, not long enough for substantial soil development, and hence why no clear temporal hiatus between the eruptions is evident in the near-source record (Table 3).

The SG14–4032 cryptotephra is preserved 1.2 m beneath the ACP4 lower unit shows a good overlap with the evolved member of the ACP6 tephra preserved NE of the caldera at Koga (Fig. 7C). Glasses from both the SG14–4032 and ACP6 tephra deposits are relatively distinctive at the trace element level owing to their SiO_2, CaO and Sr contents (Fig. 5A, 7E) and are preserved in the same stratigraphic position, above the widespread Kuju-Hd/P1 marker, that is equivalent to to the SG06–4141/SAN1 marine tephra. Based on the good chrono-stratigraphic and geochemical agreement, we correlate the SG14–4032 to the ACP6 unit at Koga, and refine the age of the eruption to 51.5 ± 1.0 ka using the Lake Suigetsu age-depth model. This age is ~8 kyrs younger than the ACP6 age estimate presented by Miyabuchi (2009), which was based on radiocarbon dating of interbedded palaeosols.

In the 8.0 m of Lake Suigetsu sediments between the Aso-4 (SG06–4963) and ACP6 (SG14–4032) eruption deposits there are four Aso derived cryptotephra: SG14–4135, SG14–4159, SG14–4352, and SG14–4471 (Table 3). These four deposits span a 13 kyr interval and based on their chrono-stratigraphic position are likely to relate to a series of eruptions deposits known as the Yamasaki Pumices (1 to 13) (Fig. 2). Glasses from SG14–4352 show the greatest affinity with the Yamasaki pumice and ash fall units analysed (Fig. 7G-H). Specifically, SG14–4352 shows geochemical overlap with the glasses from the YmP5 eruption unit, yet also some overlap with the older YmP6 (Fig. 7G-H). The YmP5 tephra is the thickest Yamasaki pumice eruption deposits, comprising of lower pumice- and ash fall beds, and an upper scoria-fall, whereas the older YmP6 unit is a single thin pumice layer (Miyabuchi, 2009; Miyabuchi et al., 2003). Here, only the lower pumice fall of the YmP5 was sufficiently well preserved for glass analysis. Given that the upper portion of the YmP5 is comprised of scoria, its distal equivalent is likely to span a greater geochemical range than the YmP5 pumice sample analysed. The YmP5 is believed to have erupted over a relatively short period, and is identified as the key post-caldera marker layer. Its ENE dispersal trajectory (Miyabuchi, 2009) suggests a potential dispersal towards Lake Suigetsu 525 km away. Due to the geochemical agreement and the known dispersal axis, we provisionally correlate the SG14–4352 tephra to the YmP5 eruption unit and revise the age of this eruption to 64.1 ± 2.4 ka using the Lake Suigetsu age-depth model (Table 3). Whilst we are unable to correlate the three cryptotephra deposits (SG14–4032, SG14–4135 and SG14–4159) preserved above and the one (SG14–4471) below the YmP5 (SG14–4352) in Lake Suigetsu to specific Aso eruptions using our proximal geochemical data, we suggest that these may be the distal deposits of eruptions in the remaining YmP1 to 4 and YmP9 to 13 series, respectively. These eruptions have not been geochemically characterised due to poor glass preservation. Due to the occurrence of the YmP5 and ACP6 tephras in Lake Suigetsu, we can constrain the ages for the YmP1 to 4 eruptive deposits to between 64.1 and 51.5 ka. Likewise, the occurrence of Aso-4 and YmP5 at Lake Suigetsu allows us to constrain the YmP6 to 13 eruptive deposits, and the NjP eruption to between 86 ka and 64.1 ka (Table 3). Given that the Yamasaki pumice series deposits are so weathered, it is unlikely that more eruption specific correlations with the Lake Suigetsu ashfall record can be established. However, our data clearly indicate that this period of eruptive activity at the volcano was responsible for multiple widespread ashfall events.

5.3. Pre-Aso-4

Of the six Aso eruption deposits preserved beneath Aso-4 in Lake Suigetsu, three can be correlated with proximal counterparts (Table 3). These Aso cryptotephra deposits are located between the previously identified Aso-ABCD (SG06–5287) and Aso-4 (SG06–4963) visible tephra layers preserved at Lake Suigetsu: SG14–5071, SG14–5099 and SG14–5221 (Table 3). These three deposits chrono-stratigraphically correspond to the Stage 5 activity at Aso as reported by Hoshizumi et al. (2022), and these cryptotephra deposits all have shard concentrations exceeding 20,000 shards/g (Table 3). Both the SG14–5071 and SG14–5099 cryptotephra deposits are preserved in the 0.7 m of sediment above the K-Tz (SG06–5181) deposit in Lake Suigetsu, and the SG14–5221 is identified 0.8 m beneath the K-Tz (Vineberg et al., 2024). Whilst the Aso-Y tephra is preserved in proximal sequences in the same chrono-stratigraphic position as the SG14-5071 and SG14–5099 cryptotephra deposits (between the K-Tz and Aso-4 markers; Fig. 3), analyses presented in Vineberg et al. (2024) revealed that these cryptotephra layers have lower K_2O contents than the previously published Aso-Y glasses (Fig. 8A) and thus do not correlate. The new near-source glass data for Aso-Y presented here extends the compositional range, but the Lake Suigetsu tephra deposits in the same chrono-stratigraphic position still do not exhibit the same glass chemistry.

The SG14–5071 cryptotephra is preserved 1.5 m beneath the 3.5 cm thick Aso-4 tephra (SG06–4963) at Lake Suigetsu, sedimentation rates indicate that SG14-5071 former predates the Aso-4 caldera-forming event by ~5 kyr, with the cryptotephra dated at Lake Suigetsu to 91.2 ± 1.8 ka. The glass chemistry of SG14–5071 is similar to the most evolved component 1 of the Aso-4 PDC deposits, and the newly characterised Aso-4X glasses, both at a major and trace elements level (Fig. 8A-B). Although, there is a minor offset between the K_2O content of the proximal units and the distal cryptotephra. In terms of establishing the source correlative of the SG14–5071 cryptotephra there appears two possibilities; the first is that SG14–5071 is the distal correlative of the Aso-4X eruption unit, supported by the overall compositional agreement and its stratigraphic positioning below the Aso-4 PDCs, both proximally and distally at Lake Suigetsu (SG06–4963). This interpretation would infer that the Aso-4X Plinian fall unit is not directly associated with the Aso-4 caldera-forming eruption as previously proposed by Hoshizumi et al. (2022), and instead equates to a temporally separate eruption, occurring 5 kyr prior to the Aso-4 eruption. While there is no palaeosol observed between the Aso-4X and Aso-4 deposit at Kurumibaru (AS10042), there is a sharp erosional unconformity at the top of the Aso-4X fall, indicating the erosive power of the Aso-4 PDCs could have removed evidence of a time gap between the Aso-4X and the caldera-forming event. The alterative scenario is that the Aso-4X unit is indeed the Plinian fall phase of the Aso-4 caldera-forming eruption as proposed by Hoshizumi et al. (2022), and the SG14–5071 cryptotephra is unrelated to the Aso-4X eruption unit, but instead evidences yet another pre-Aso-4, compositionally similar, eruptive event that has been eroded out by the Aso-4 PDCs in the sections investigated. For the moment we are unable to conclusively attribute SG14–5071 to the Aso-4X, but in either scenario the Lake Suigetsu ashfall record indicates that the voluminous PDC associated with this caldera-forming event has removed at least some of the near-source eruption record immediately prior to this

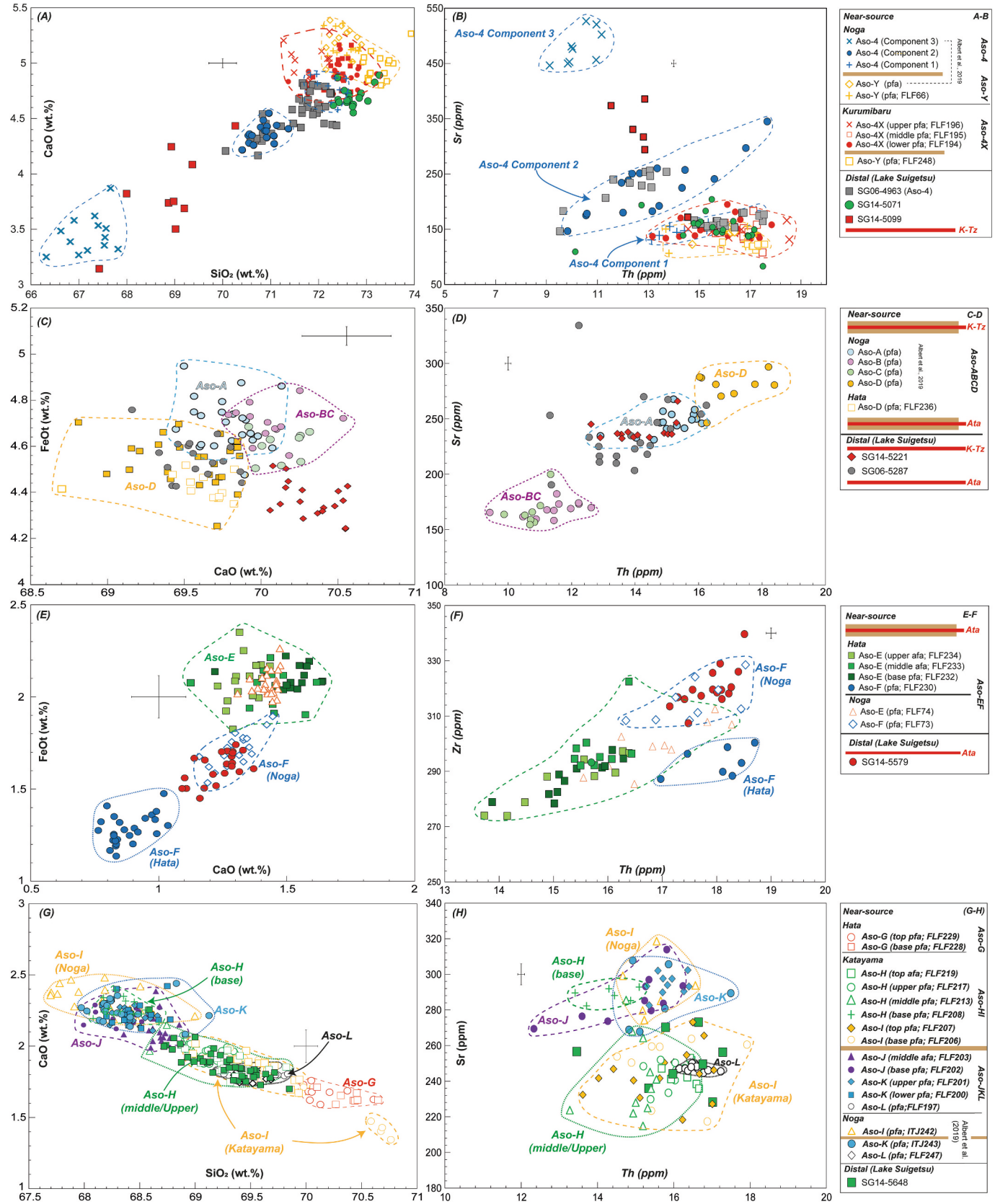

Fig. 8. Major (WDS-EMP) and trace element (LA-ICP-MS) glass compositions of the Aso crypto−/tephra deposits preserved between the Aso-3 and Aso-4 tephra layers in the Lake Suigetsu sequence compared to reference chemical datasets produced for chrono-stratigraphically relevant eruption units. Reference chemical datasets obtained from proximal outcrops are from: This Study; McLean et al., 2020 and Albert et al., 2019a. Error bars represent 2 x standard deviation of repeat analyses of the StHs6/80-G MPI-DING standard glass.

catastrophic eruption. Indeed, evidence for the erosive nature of the Aso-4 PDCs is observed at Hata, where the Aso-4 PDC deposits cuts down through to the Aso-D fall deposit removing the overlying tephra (Fig. 3), and all the deposits of Stage 5 activity.

The SG14–5221 sits 30 cm stratigraphically above the 3.5 cm thick visible SG06–5287 tephra that has been correlated with Aso-ABCD eruption (Albert et al., 2019a; Smith et al., 2013). The SG06–5287 glasses were tentatively correlated with those of the Aso-A sub-unit owing to similarities in Y and Th contents (Albert et al., 2019a). Although SG14–5221 glasses show compositional overlap with both the Aso-A sub-unit and SG06–5287 at the trace element level (Fig. 8B), they display lower K_2O contents (Fig. 8A). Thus, perhaps suggesting that SG14–5221 corresponds to a younger post-Aso-ABCD eruption.

Based on our asessment of tephra correlations to the Lake Suigetsu record, the 10 kyr time-window between the Aso-ABCD and leading up to the Aso-4 caldera-forming event (Stage 5; Hoshizumi et al., 2022) is unlikely to be restricted to a single eruptive event (Aso-Y), our distal data present important evidence for eruption under-recording in the near-source setting.

Here new near-source glass geochemical data has facilitated the correlation of two additional distal Lake Suigetsu tephra deposits to Stage 4: Aso-EF and Aso-HI. In the 4.2 m of sediment beneath the Aso-ABCD tephra (SG06–5287), Vineberg et al. (2024) identified two Aso tephra deposits, SG14–5579 and SG14–5648, dated to 108.4 ± 4.0 ka and 110.8 ± 4.2 ka, respectively (Table 3). Both deposits are preserved beneath the widespread tephra markers, Ata at 100 ka from Ata caldera (southern Kyushu), the SK tephra from Sambe volcano (SW Honshu) and the Toya tephra from Toya caldera (southern Hokkaido), in the Lake Suigetsu (see Fig. 9).

The glasses from the 0.8 cm thick SG14–5579 visible tephra are distinct from other Aso glasses preserved in Lake Suigetsu at the trace element level owing to a higher Th population (Fig. 4D). The SG14–5579 glasses show a clear geochemical affinity with the chrono-stratigraphically relevant Aso-F pumice fall glasses sampled at Noga, most notably both displaying high Th and Zr contents not present in any other pre-Ata geochemically analysed Aso units (Fig. 8E-F). We therefore determine the SG14–5579 cryptotephra preserved in Lake Suigetsu represents the distal equivalent to the Aso-EF eruptive deposits, and revise the age for this M 5.2 eruption to 108.4 ± 4.0 ka, which is significantly older than the 99.2 ka estimate by Hoshizumi et al. (2022) based on loess-chronometry. The Lake Suigetsu age-model indicates a period of ~12 kyr elapsed between the Aso-EF and subsequent Aso-ABCD eruption, which is consistent with the stratigraphic position of the Ata tephra (Albert et al., 2019a; Hoshizumi et al., 2022) within the palaeosol developed between the two deposits at Noga (Fig. 3).

The SG14–5648 cryptotephra is the first post Aso-3 tephra preserved in Lake Suigetsu and is found 69 cm beneath the Aso-EF (SG14–5579) tephra. It has a high shard concentration of >20,000 shards/g (Table 3). Vineberg et al. (2024) reported a similarity of the SG14–5648 glasses with those of the Aso-I eruption unit (Albert et al., 2019a). The new more extensive major element dataset here confirm a compositional overlap with the Aso-HI eruptive deposits, but also indicate an overlap with the older Aso-L glasses (from the preceding Aso-JKL eruption) (Fig. 8G). Overall, the Aso-L sub-unit analysed is distinct from the overlying Aso-K and Aso-J sub-units, and has a very homogeneous glass composition (Fig. 8H). In contrast the distal cryptotephra SG14–5648 has a greater degree of heterogeneity, more consistent with the Aso-HI deposits. Indeed, using the Th vs. Sr bi-plot, the SG14–5648 cryptotephra glasses show better agreement with the glasses of the Aso-HI eruption deposits (Fig. 8H). Thus, the SG14–5648 cryptotephra is considered the distal equivalent of the Aso-HI eruption with an age of 110.8 ± 4.2 ka, which is older than the 102.6 ka estimate by Hoshizumi et al. (2022).

5.4. Aso integrated near-source and distal eruption record: implications

Integrating near-source and distal eruption records is critical to addressing inherent gaps in the proximal eruption record. This requires detailed chemical fingerprinting of available near-source records and distal tephra layers preserved in sedimentary archives. At Aso volcano, the potential for erroneous tephra correlations between near-source sections has been highlighted by the often similar or overlapping geochemical signatures of the eruption deposits investigated, with this having implications for distal tephra correlations. However, the data here have highlighted the benefits of adopting a detailed glass geochemical fingerprinting approach to test near-source tephrostratigraphic correlations, with analysis revealing chemo-stratigraphic discrepancies between eruption units or phases. For instance with respect to the Aso-HI eruption, the Aso-I pumice fall deposits at Noga and Katayama have different volcanic glass signatures (Fig. 6), with the former more akin to the overlying Aso-H eruptive products, this can be used to infer that the opening phase of the Aso-HI eruption was dispersed to the SE (and not preserved at Noga), before the plume migrated towards the north during the eruption (depositing Aso-H, which is preserved at both localities). The overlapping Aso chemical signatures also reinforce the importance of a robust chrono-stratigraphic framework when integrating the near-source eruption deposits with those preserved in distal sedimentary records such as Lake Suigetsu. Stratigraphic constraints, coupled with detailed chemical analysis, have meant that the distal record has helped distinguish geochemically similar, but temporally distinct eruptive units, thereby refining the eruption frequency of Aso (e.g., ACP4). Fortunately, many of the volcanic deposits are interspersed between key tephra layers from other Japanese volcanic sources, both in the near-source setting, and in the Lake Suigetsu sedimentary sequence (Fig. 9), which aid the tephra correlations and will facilitate future synchronisation with other tephra records. For instance, the YmP5 tephra is preserved below the widespread DSP tephra from Daisen volcano, and the Aso-EF and Aso-HI tephra deposits are beneath the tephra deposits of the Ata and Toya caldera-forming eruptions (Fig. 9). The integration of the Aso proximal stratigraphy with the Lake Suigetsu record, a key tephro-stratotype for East Asia, is critical to providing age constraints of the source eruptions, deposits that are not easily directly dated using radiometric dating methods.

Nine of the Aso tephra deposits recognised in near-source outcrops between the Aso-3 and AT eruption deposits have been identified 525 km northeast of the volcano in the Lake Suigetsu sedimentary sequence. These eruptions include the Aso-Kpfa, Upper ACP4, Lower ACP4, ACP6, YmP5, Aso-4, Aso-ABCD, Aso-EF and Aso-HI (Table 3; Fig. 9). Six of these correlations have been facilitated through the new near-source volcanic glass chemical data presented here. The Lake Suigetsu age-depth model has constrained the ages of Aso ashfall deposits. These include the newly identified tephra and cryptotephra deposits associated with the Upper ACP4 (48.7 ± 0.2 ka), Lower ACP4 (49.1 ± 0.2 ka), ACP6 (51.5 ± 1.0 ka), YmP5 (64.1 ± 2.4 ka), Aso-EF (108.4 ± 4.0 ka), and Aso-HI (110.8 ± 4.2 ka; Table 3). These ages are broadly consistent with earlier estimates for some of these eruptions, others have been further constrained (Tables 1, 3). Importantly, the Lake Suigetsu age-depth model also provides age constraints for those remaining distal Aso tephra layers not yet recognised in the near-source record (Table 3). This integration also offers key insights into the frequency, scale and dispersal of past eruptions in the lead up to and following caldera eruptions.

The eruptions that produced the twenty Aso volcanic deposits within Lake Suigetsu are likely to be ≥ M5.0 in order to have dispersed tephra 525 km away from source (c.f. Sulpizio et al., 2024). Indeed, the Lake Suigetsu ashfall record captures the distal tephra from the largest of the

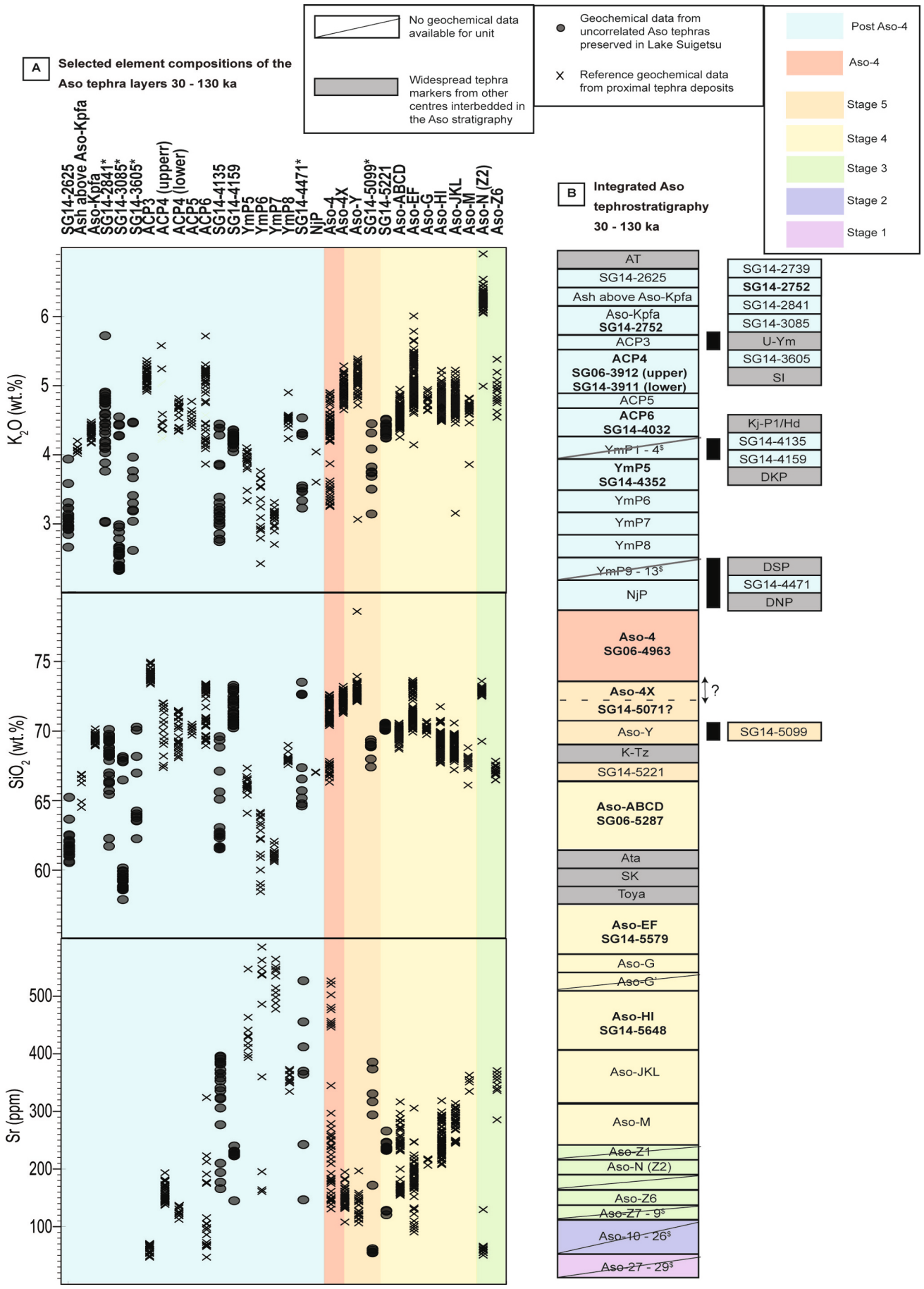

(caption on next page)

Fig. 9. (A) Selected major and trace elements useful for recognising variations in the volcanic glasses erupted from tephra units preserved between the Aso-3 (~130 ka) and AT (~30 ka) tephras in outcrops around the caldera (black crosses) as well as uncorrelated Aso tephras identified in the Lake Suigetsu archive (black circles) which have been geochemically analysed. * represents units with stratigraphic positions that are not precisely constrained and may, for example be 1 unit too high, or 3 too low. $ represents multiple units. Data for these units are from: This Study; McLean et al., 2020; Albert et al., 2019a; Smith et al., 2013). **(B)** An integrated proximal-distal stratigraphy of Aso eruptions based on proximal outcrops and Lake Suigetsu tephra record. The black bar represents the relative stratigraphic position of Lake Suigetsu Aso tephra layers where their precise position in the near-source record is unclear. The height of boxes is indicative of the magnitude of eruption (i.e. larger boxes represent higher magnitude eruptions). Stages 1–5 are as defined by Hoshizumi et al. (2022).

post-Aso-4 eruptive units, Aso-Kpfa, ACP4, ACP6 and YmP5 (Miyabuchi et al., 2003, 2009). The discovery that two distal ash fall deposits associated with ACP4 activities are preserved at Lake Suigetsu, separated by ~400 years of sedimentation, has important implications for magnitude-frequency estimates. Temporally dividing some of the near-source deposits into separate events might infer that that the erupted volume and magnitude are slightly lower. However, despite the apparent grouping of the near-source ACP4 deposits into a single eruption (tephra volume 0.43 km^3; Miyabuchi, 2009), by applying the simplified two locality tephra volume calculation of Sulpizio et al. (2024), the Upper ACP4 (Koga) fall (17 cm thickness; $d0 = 15$ km) deposit, and the distal equivalent at Lake Suigetsu, visible tephra SG06–3912 (0.1 cm thickness; $d1 = 525$ km), would indicate an average minimum tephra volume of 6.21 km^3, which corresponds to M5.8. While the Lower ACP4 is only preserved as a cryptotephra at Lake Suigetsu, and is not suitable for such a calculation, given similar near-source thicknesses, it would imply that the two ACP4 eruptions have independently erupted tephra volumes that exceed the combined near-source volume estimate for the ACP4 deposits. Furthermore, the identification of the ACP6 ash fall in Lake Suigetsu revises the eruption age of this earlier Plinian eruption to 51.5 ± 1.1 ka (1σ), younger than previous age estimates (~60 ka; Miyabuchi, 2009). With ACP6 now dated to 51.5 ± 1.1 ka this provides further constraints on the frequency of activity at the central cones of Aso during this time interval. The integrated age information indicates a clustering of least four Plinian eruptions occurred between 52 and 48 ka (ACP6, ACP5, Lower ACP4 and Upper ACP4), with the age of a fifth the Plinian ACP3 fall slightly younger, still only loosely constrained by its chrono-stratigraphic association to the 51.0 ± 5.0 ka Takanoobane lava (Matsumoto et al., 1991; Miyabuchi, 2009).

Furthermore, in relation to the pre-Aso-4 activity and Stage 4, the Aso-ABCD and Aso-HI eruption deposits preserved within the Lake Suigetsu sediments represent the two largest eruptions, M5.9 and M5.7, respectively (Hoshizumi et al., 2022). In addition, the visible (0.8 cm thick) tephra SG14–5579 is correlated with the Aso-F (Noga, 30 cm) fall deposit, according to the method of Sulpizio et al. (2024), this would indicate the Aso-EF eruption had an average minimum volume of 8.26 km^3, equivalent to M5.9, perhaps inferring a higher erupted volume and magnitude than previously estimated for this eruption (Table 1).

There are eleven Aso deposits preserved within the Lake Suigetsu sediments that we have not yet been able to correlate to a specific eruption units defined proximally. Although three of these distal layers (SG14–4471, SG14–4159 and SG14–4135) are in stratigraphic positions where there are recorded Aso eruption deposits (Yamasaki pumices), there are six distal layers (SG14–2625, SG14–2841, SG14–3085, SG14–3605, SG14–5099 and SG14–5221) preserved within Lake Suigetsu that are from stratigraphic positions where there are no prominent units are preserved in the proximal exposures that have been studied. This might suggest that the exposures available may be incomplete. This is particularly relevant to the pre-Aso-4 interval and specifically Stage 5, where during the ~10 kyrs prior to the Aso-4 caldera-forming eruption, proximally only the Aso-Y eruption deposit is identified (Hoshizumi et al., 2022), yet at least two (SG14–5099 and SG06–5221) distal tephra fall deposits, perhaps a third (SG14–5071?) have been resolved at Lake Suigetsu. This highlights that large caldera-forming eruptions erode or conceal the near-source eruption record produced in the lead up to these large magnitude events.

Several of the eruptions reported from outcrops to the east of the caldera wall are not preserved within Lake Suigetsu (e.g. ACP3, ACP5, Aso-Y and Aso-G) indicating that they were likely either smaller eruptions, or their ash dispersals were incompatible with deposition and preservation to the NE at the Lake Suigetsu (Table 1). Moreover, although most major silicic activity at Aso occurred pre-30 ka, eruptions have been reported above the AT tephra in near-source outcrops (Miyabuchi, 2009). Yet none of these post-AT Aso eruptions have been identified within the Lake Suigetsu sediments (see Albert et al., 2024, 2019a; McLean et al., 2018, Smith et al., 2013), despite some of the more recent eruptions also having an ENE dispersal. The fact that they are not preserved at Lake Suigetsu must presumably be due to their smaller ejected tephra volumes (<1.0 km^3), which correspond to a M of ≤3.0. This study would indicate that at sites >500 km from the eruption source, cryptotephra can be preserved in sedimentary records, particularly if the total erupted tephra volume exceeds 1 km^3 (i.e., >M3.0). Lake Suigetsu is positioned favourably along the general dispersal axis from Aso, which refers to the dominant transport pathway of volcanic ash controlled by prevailing westerly wind patterns and eruption dynamics. These findings suggest that in a suitable depositional settings even moderate-sized eruptions can contribute detectable cryptotephra deposits at considerable distances from the volcanic source. This research highlights the relationship between eruption size, dispersal distance and trajectory, and the potential for preserving volcanic ash in sedimentary records, which are essential for reconstructing high-resolution volcanic histories.

6. Conclusions

In this study, we summarise the explosive volcanic activity of Aso volcano between 130 and 30 ka and provide glass compositional data for the largest and likely most widespread eruption deposits. Volcanic glass geochemistry reveals several Aso eruption units display similar or overlapping major element chemistries, demonstrating the importance of utilising detailed geochemical analysis, integrated within a detailed tephrostratigraphic framework, to robustly correlate near-source and distal tephra deposits. With this new data, we integrate the near-source Aso eruption record with the Aso derived tephra deposits preserved in the Lake Suigetsu sedimentary record, these now include: Aso-Kpfa, Upper ACP4 and Lower ACP4, ACP6, YmP5, Aso-4, Aso-ABCD, Aso-EF and Aso-HI. These correlations provide invaluable chronological constraints for these eruptions, including insights into the tempo of activity, and the ash dispersals. Most of the Lake Suigetsu tephra layers correlated with the known near-source counterparts originate from some of the largest pre- and post- Aso-4 eruptions. These eruptions produced considerable tephra volumes (>1.7 km^3), allowing for widespread dispersal of volcanic ash across large geographical areas of Japan. As a result, they serve as valuable markers for synchronizing distal records (e.g., Aso-HI, Aso-ABCD, ACP4, and Aso-Kpfa). Furthermore, the identification of an additional Aso tephras in Lake Suigetsu provides better age constraints for these eruptions and thus allows a refined understanding of the tempo of activity. For example, a consequence of identifying the ACP6 in Lake Suigetsu, it means that the ACP6, ACP5, Lower ACP4 and Upper ACP4 Plinian eruptions from the Aso central cones occurred within a ~ 4 kyr period. Furthermore, the potential to geochemically distinguish the upper and lower units of the ACP4 fall deposits have enabled both to be identified as temporally distinct layers at Lake Suigetsu, revealing that ~400 years occurred between these Plinian eruptions. The previous grouping of these eruption deposits as a single events

has implications for frequency-magnitude relationships. The Lake Suigetsu ashfall record has also elucidated a greater number of Aso explosive eruptions in the 10 kyrs leading up to the Aso-4 caldera-forming eruption, particularly when contrasted with the near-source record. Similarly, at least two eruptions occur shortly after the Plinian Aso-Kpfa eruption which are not clearly preserved in the near-source record, and again illustrating a clustering of eruptions at the volcano. Overall, this research expands the glass geochemical database for Aso tephra deposits. Furthermore, these glass data facilitate the integration of the proximal-distal record, updating the tephrostratigraphic framework for one of the world's most active calderas. Future studies should be undertaken to capitalise on distal ashfall records to better constrain the timing, magnitude and dispersal of past eruptions, in order to inform future hazard and risk management strategies.

CRediT authorship contribution statement

Sophie O. Vineberg: Writing – review & editing, Writing – original draft, Visualization, Resources, Methodology, Investigation, Funding acquisition, Formal analysis, Data curation, Conceptualization. **Paul G. Albert:** Writing – review & editing, Validation, Supervision, Resources, Methodology, Funding acquisition, Formal analysis, Data curation, Conceptualization, Project administration, Visualization. **Danielle McLean:** Writing – review & editing, Data curation, Conceptualization. **Takehiko Suzuki:** Resources, Data curation. **Yasuo Miyabuchi:** Visualization, Resources, Data curation. **Hideo Hoshizumi:** Visualization, Resources, Data curation. **Hannah M. Buckland:** Resources, Data curation. **Gwydion Jones:** Data curation. **Fumikatsu Nishizawa:** Data curation. **Richard A. Staff:** Writing – review & editing, Formal analysis. **Keitaro Yamada:** Writing – review & editing, Resources. **Ikuko Kitaba:** Resources. **Junko Kitagawa:** Resources. **Christina J. Manning:** Resources. **Takeshi Nakagawa:** Resources, Funding acquisition. **Victoria C. Smith:** Writing – review & editing, Supervision, Resources, Funding acquisition, Data curation, Conceptualization.

Declaration of competing interest

The authors declare that they have no known competing financial interests or personal relationships that could have appeared to influence the work reported in this paper.

Acknowledgements

S.O.V. is funded by NERC as part of the Environmental Research Doctoral Training Programme at the University of Oxford (NERC; NE/S007474/1). This research was funded through a UKRI Future Leaders Fellowship (FLF) awarded to P.G.A (MR/S035478/1 and MR/Y011767/1), which also supported D.M., H.M.B and G.J. Furthermore, V.C.S and T.N. acknowledge funding from the Japan Society for the Promotion of Science (JSPS; KAKENHI-15H021443). The SG06 coring campaign was funded by the UK Natural Environmental Research Council (NERC; NE/D000289/1) New Investigators Award to T.N. The Fukui-SG14 coring campaign was funded by the Fukui Prefectural government, Japan. T.S. acknowledges funding from the Japan Society for the Promotion of Science (JSPS; KAKENHI-22H02380). D.M was supported by a Leverhulme Early Career Fellowship (ECF-2020-151) and the John Fell Fund (#9438) at the University of Oxford. F.N. acknowledges funding from the Japan Society for the Promotion of Science (JSPS; KAKENHI-JP19K13438. The Lake Suigetsu coring was conducted by the team of Seibushisui Co. Ltd. Japan, led by Mr. Atsumi Kitamura. Chris Hayward is thanked for his support at the Tephra Analysis Unit, University of Edinburgh. We would also like to thank an Anonymous Reviewer and Prof. Roberto Sulpizio for their constructive comments which improved the manuscript, and Prof. Ed Llewellin for editorial handling.

Appendix A. Supplementary data

Supplementary data to this article can be found online at https://doi.org/10.1016/j.jvolgeores.2025.108436.

Data availability

All geochemical data are provided in the Suplementary data files.

References

Albert, P.G., Smith, V.C., Suzuki, T., Tomlinson, E.L., Nakagawa, T., McLean, D., Yamada, M., Staff, R. A, Schlolaut, G., Takemura, K., 2018. Constraints on the frequency and dispersal of explosive eruptions at Sambe and Daisen volcanoes (South-West Japan Arc) from the distal Lake Suigetsu record (SG06 core). Earth Sci. Rev. 185, 1004–1028. https://doi.org/10.1016/j.earscirev.2018.07.003.

Albert, P.G., Smith, V.C., Suzuki, T., McLean, D., Tomlinson, E.L., Miyabuchi, Y., Kitaba, I., Mark, D.F., Moriwaki, H., Nakagawa, T., 2019a. Geochemical characterisation of the late Quaternary widespread Japanese tephrostratigraphic markers and correlations to the Lake Suigetsu sedimentary archive (SG06 core). Quat. Geochronol. https://doi.org/10.1016/j.quageo.2019.01.005.

Albert, P.G., Giaccio, B., Isaia, R., Costa, A., Niespolo, E.M., Nomade, S., Pereira, A., Renne, P.R., Hinchliffe, A., Mark, D.F., Brown, R.J., Smith, V.C., 2019b. Evidence for a large-magnitude eruption from Campi Flegrei caldera (Italy) at 29 ka. Geology 47, 595–599.

Albert, P.G., McLean, D., Buckland, H.M., Suzuki, T., Jones, G., Staff, R.A, Vineberg, S., Kitaba, I., Yamada, K., Moriwaki, H., Ishimura, D., Ikehara, K., Manning, C.J., Nakagawa, T., Smith, V.C., 2024. Cryptotephra preserved in Lake Suigetsu (SG14 core) reveals the eruption timing and distribution of ash fall from Japanese volcanoes during the Late-glacial to early Holocene. Quat. Sci. Rev. 324, 10837. https://doi.org/10.1016/J.QUASCIREV.2023.108376.

Aoki, K., 2008. Revised age and distribution of ca. 87 ka Aso-4 tephra based on new evidence from the Northwest Pacific Ocean. Quat. Int. 178 (1), 100–118. https://doi.org/10.1016/j.quaint.2007.02.005.

Bourne, A.J., Lowe, J.J., Trincardi, F., Asioli, A., Blockley, S.P.E., Wulf, S., Matthews, I. P., Piva, A., Vigliotti, L., 2010. Distal tephra record for the last ca 105,000 years from core PRAD 1-2 in the Central Adriatic Sea: implications for marine tephrostratigraphy. Quat. Sci. Rev. 29 (23–24), 3079–3094.

Bronk Ramsey, C., 2008. Deposition models for chronological records. Quat. Sci. Rev. 27 (1–2), 42–60. https://doi.org/10.1016/j.quascirev.2007.01.019.

Bronk Ramsey, C., Heaton, T.J., Schlolaut, G., Staff, R.A., Bryant, C.L., Brauer, A., Lamb, H.F., Marshal, M.H., Nakagawa, T., 2020. Reanalysis of the atmospheric radiocarbon calibration record from Lake Suigetsu, Japan. Radiocarbon 62 (4). https://doi.org/10.1017/RDC.2020.18.

Bronk Ramsey, C., Staff, R.A, Bryant, C.L., Brock, F., Kitagawa, H., Van Der Plicht, J., Schlolaut, G., Marshall, M.H., Brauer, A., Lamb, H.F., Payne, R.L., 2012. A complete terrestrial radiocarbon record for 11.2 to 52.8 kyr BP. Science 338 (6105), 370–374. https://doi.org/10.1126/science.1226660.

Chun, J.H., Ikehara, K., Sang-Joon, H., 2004. Evidence in Ulleung Basin sediment cores for a Termination II (penultimate deglaciation) eruption of the Aso-3 tephra. The Quaternary Research (Daiyonki-Kenkyu) 43 (2), 99–11.

Davies, S.M., Albert, P.G., Bourne, A.J., Owen, S., Svensson, A., Bolton, M.S., Cook, E., Jensen, B.J., Jones, G., Ponomareva, V.V., Suzuki, T., 2024. Exploiting the Greenland volcanic ash repository to date caldera-forming eruptions and widespread isochrons during the Holocene. Quat. Sci. Rev. 334, 108707.

de Maisonneuve, C.B., Forni, F., Bachmann, O., 2021. Magma reservoir evolution during the build up to and recovery from caldera-forming eruptions–a generalizable model? Earth Sci. Rev. 218, 103684.

Derkachev, A.N., Utkin, I.V., Nikolaeva, N.A., Gorbarenko, S.A., Malakhova, G.I., Portnyagin, M.V., Sakhno, V.G., Shi, X., Lv, H., 2019. Tephra layers of large explosive eruptions of Baitoushan/Changbaishan Volcano in the Japan Sea sediments. Quat. Int. 519, 200–214. https://doi.org/10.1016/J.QUAINT.2019.01.043.

Fernandez, G., Giaccio, B., Costa, A., Monaco, L., Nomade, S., Albert, P.G., Pereira, A., Flynn, M., Leicher, N., Lucchi, F., Petrosino, P., 2024. New constraints on the Middle-late Pleistocene Campi Flegrei explosive activity and Mediterranean tephrostratigraphy (~ 160 ka and 110–90 ka). Quat. Sci. Rev. 331, 108623.

Hayward, C., 2012. High spatial resolution electron probe microanalysis of tephras and melt inclusions without beam-induced chemical modification. The Holocene 22 (1), 119–125.

Hoshizumi, H., Miyabuchi, Y., Miyagi, I., Geshi, N., Takarada, S., 2022. Tephrostratigraphy and eruptive history of Aso-4/3 tephra group, Aso volcano: preparatory process for Aso-4 ignimbrite eruption. Bull. Volcanol. Soc. Jpn. 67 (1), 91–112.

Hoshizumi, H., Takarada, S., Miyabuchi, Y., Miyagi, I., Yamasaki, T., Kaneda, Y., Geshi, N., 2023. Distribution Map of Aso-4 Ignimbrite and Associated Deposits, Aso Caldera, Japan. Distribution Map of Large-Volume Ignimbrites in Japan, no.3, Geological Survey of Japan. AIST, 35p.

Hoshizumi, H., Takarada, S., Miyabuchi, Y., Miyagi, I., Yamasaki, T., Kaneda, Y., Geshi, N., 2024. Distribution Map of Aso-3 Ignimbrite and associated deposits, Aso Caldera, Japan. In: Distribution Map of Large-volume Ignimbrites in Japan, no.4, Geological survey of Japan. AIST, 27p.

Ikehara, K., 2015. Marine tephra in the Japan Sea sediments as a tool for paleoceanography and paleoclimatology. Prog. Earth Planet. Sci. 2 (1), 1–14. https://doi.org/10.1186/S40645-015-0068-Z.

Jochum, K.P., Stoll, B., Herwig, K., Willbold, M., Hofmiann, A.W., Amini, M., Aarburg, S., Abouchami, W., Hellebrand, E., Mocek, B., Raczek, I., Stracke, A., Alard, O., Bouman, C., Becker, S., Dücking, M., Brätz, H., Klemd, R., De Bruin, D., Woodhead, J.D., 2006. MPI-DING reference glasses for in situ microanalysis: new reference values for element concentrations and isotope ratios. Geochem. Geophys. Geosyst. 7 (2). https://doi.org/10.1029/2005GC001060.

Kaneko, K., Inoue, K., Koyaguchi, T., Yoshikawa, M., Shibata, T., Takahashi, T., Furukawa, K., 2015. Magma plumbing system of the Aso-3 large pyroclastic eruption cycle at Aso volcano, Southwest Japan: petrological constraint on the formation of a compositionally stratified magma chamber. J. Volcanol. Geotherm. Res. 303, 41–58. https://doi.org/10.1016/J.JVOLGEORES.2015.07.016.

Keller, F., Guillong, M., Geshi, N., Miyakawa, A., Bachmann, O., 2023. Tracking caldera cycles in the Aso magmatic system–applications of magnetite composition as a proxy for differentiation. J. Volcanol. Geotherm. Res. 436, 107789.

Kiyosugi, K., Connor, C., Sparks, R.S.J., Crosweller, H.S., Brown, S.K., Siebert, L., Wang, T., Takarada, S., 2015. How many explosive eruptions are missing from the geologic record? Analysis of the quaternary record of large magnitude explosive eruptions in Japan. J. Appl. Volcanol. 4 (1), 1–15. https://doi.org/10.1186/S13617-015-0035-9, 2015 4:1.

Lane, C.S., Chorn, B.T., Johnson, T.C., 2013. Ash from the Toba supereruption in Lake Malawi shows no volcanic winter in East Africa at 75 ka. Proc. Natl. Acad. Sci. 110 (20), 8025–8029.

Lim, C., Toyoda, K., Ikehara, K., Peate, D.W., 2013. Late Quaternary tephrostratigraphy of Baegdusan and Ulleung Volcanoes using marine sediments in the Japan Sea/East Sea. Quat. Res. 80 (1), 76–87. https://doi.org/10.1016/J.YQRES.2013.04.002.

Machida, H., 2002. Volcanoes and tephras in the Japan area. Glob. Environ. Res. English Ed. 6 (2), 19–28.

Machida, H., Arai, F., 1994. Implications of the time-marker Aso-3 tephra to the significant lowering of sea level in the marine isotope stage 5d. J. Geogr. (Chigaku Zasshi) 103 (7), 749–759.

Machida, H., Arai, F., 2003. Atlas of Tephra in and around Japan, New edition (in Japanese).

Mahony, S.H., Sparks, R.S.J., Wallace, L.M., Engwell, S.L., Scourse, E.M., Barnard, N.H., Kandlbauer, J., Brown, S.K., 2016. Increased rates of large-magnitude explosive eruptions in Japan in the late Neogene and Quaternary. Geochem. Geophys. Geosyst. 17 (7), 2467–2479.

Matsumoto, A., Uto, K., Ono, K., Watanabe, K., 1991. K–Ar age determinations for Aso volcanic rocks—concordance with volcanostratigraphy and application to pyroclastic flows. Programme and abstracts of the Volcanological Society of Japan 1991 (2), 73 (in Japanese).

Matsu'ura, T., Komatsubara, J., 2024. Ontake-Katamachi tephra: Marine-terrestrial correlation of a time marker of marine isotopic stage 5b in NE Japan, the Japan Sea, and the NW Pacific. J. Asian Earth Sci. 259, 10587. https://doi.org/10.1016/j.jseaes.2023.105876.

Matsu'ura, T., Furusawa, A., Shimogama, K., Goto, N., Komatsubara, J., 2014. Late Quaternary tephrostratigraphy and cryptotephrostratigraphy of deep-sea sequences (Chikyu C9001C cores) as tools for marine terrace chronology in NE Japan. Quat. Geochronol. 23, 63–79. https://doi.org/10.1016/J.QUAGEO.2014.0001.

Matsu'ura, T., Ikehara, M., Ueno, T., 2021. Late Quaternary tephrostratigraphy and cryptotephrostratigraphy of core MD012422: improving marine tephrostratigraphy of the NW Pacific. Quat. Sci. Rev. 257. https://doi.org/10.1016/j.quascirev.2021.106808.

McLean, D., Albert, P.G., Nakagawa, T., Staff, R. A, Suzuki, T., Smith, V.C., 2016. Identification of the Changbaishan 'Millennium'(B-Tm) eruption deposit in the Lake Suigetsu (SG06) sedimentary archive, Japan: synchronisation of hemispheric-wide palaeoclimate archives. Quat. Sci. Rev. 150, 301–307. https://doi.org/10.1016/j.quascirev.2017.12.013.

McLean, D., Albert, P.G., Nakagawa, T., Suzuki, T., Staff, R. A, Yamada, K., Kitaba, I., Haraguchi, T., Kitagawa, J., Smith, V., 2018. Integrating the Holocene tephrostratigraphy for East Asia using a high-resolution cryptotephra study from Lake Suigetsu (SG14 core), Central Japan. Quat. Sci. Rev. 183, 36–58. https://doi.org/10.1016/j.quascirev.2017.12.013.

McLean, D., Albert, P.G., Suzuki, T., Nakagawa, T., Kimura, J.-I., Chang, Q., MacLeod, A., Blockley, S., Staff, R. A, Yamada, K., 2020. Refining the eruptive history of Ulleungdo and Changbaishan volcanoes (East Asia) over the last 86 kyrs using distal sedimentary records. J. Volcanol. Geotherm. Res. 389, 106669. https://doi.org/10.1016/j.jvolgeores.2019.106669.

Miyabuchi, Y., 2009. A 90,000-year tephrostratigraphic framework of Aso Volcano, Japan. Sediment. Geol. 220 (3–4), 169–189. https://doi.org/10.1016/J.SEDGEO.2009.04.018.

Miyabuchi, Y., 2011. Post-caldera explosive activity inferred from improved 67-30 ka tephrostratigraphy at Aso Volcano, Japan. J. Volcanol. Geotherm. Res. 205 (3–4), 94–113. https://doi.org/10.1016/j.jvolgeores.2011.05.004.

Miyabuchi, Y., Hoshizumi, H., Takada, H., Watanabe, K., Xu, S., 2003. Pumice-fall deposits from Aso volcano during the past 90,000 years, southwestern Japan. Kazan 48 (2), 195–214.

Nagahashi, Y., Yoshikawa, S., Miyakawa, C., Uchiyama, T., Inouchi, Y., 2004a. Stratigraphy and chronology of widespread tephra layers during the past 430ky in the Kinki District and the Yatsugatake mountains major element composition of the glass shards using EDS analysis. Quat. Res. (Daiyonki-Kenkyu) 43 (1), 15–35.

Nagahashi, Y., Yoshikawa, S., Miyakawa, C., Uchiyama, T., Inouchi, Y., 2004b. Stratigraphy and chronology of widespread tephra layers during the past 430ky in the Kinki District and the Yatsugatake mountains major element composition of the glass shards using EDS analysis. Quat. Res. (Daiyonki-Kenkyu) 43 (1), 15–35.

Nagaoka, S., Okuno, M., Arai, F., 2001. Tephrostratigraphy and eruptive history of the Aira caldera volcano during 100-30 ka, Kyushu, Japan. J. Geol. Soc. Jpn. 107 (7), 432–450.

Nakagawa, T., Kitagawa, H., Yasuda, Y., Tarasov, P.E., Gotanda, K., Sawai, Y., 2005. Pollen/event stratigraphy of the varved sediment of Lake Suigetsu, central Japan from 15,701 to 10,217 SG vyr BP (Suigetsu varve years before present): description, interpretation, and correlation with other regions. Quat. Sci. Rev. 24 (14–15), 1691–1701. https://doi.org/10.1016/j.quascirev.2004.06.022.

Newhall, C.G., Self, S., 1982. The volcanic explosivity index (VEI) an estimate of explosive magnitude for historical volcanism. J. Geophys. Res. Oceans 87 (C2), 1231–1238.

Ono, K., Watanabe, K., 1983. Aso caldera. Chikyu Monthly 5 (2), 73–82.

Ono, K., Watanabe, K., 1985. Geological map of Aso volcanoes. Geol. Surv. Jpn. 4 (in Japanese).

Ono, K., Matsumoto, Y., Miyahisa, M., Teraoka, Y., Kambe, N., 1977. Geology of the Taketa district. Geol. Surv. Jpn. 145.

Pyle, D.M., 2000. Sizes of volcanic eruptions. In: Sigurdsson, H., Houghton, B.F., McNutt, S.R., Rymer, H., Stix, J. (Eds.), Encyclopedia of Volcanoes. Academic Press, London, pp. 257–264. https://doi.org/10.1016/B978-0-12-385938-9.00013-4.

Reimer, P.J., Austin, W.E.N., Bard, E., Bayliss, A., Blackwell, P.G., Bronk Ramsey, C., Butzin, M., Cheng, H., Edwards, R.L., Friedrich, M., Grootes, P.M., Guilderson, T.P., Hajdas, I., Heaton, T.J., Hogg, A.G., Hughen, K.A., Kromer, B., Manning, S.W., Muscheler, R., Palmer, J.G., Pearson, C., van der Plicht, J., Reimer, R.W., Richards, D.A., Scott, E.M., Southon, J.R., Turney, C.S.M., Wacker, L., Adophi, F., Büntgen, U., Capano, M., Fahrni, S., Fogtmann-Schulz, A., Friedrich, R., Kudsk, S., Miyake, F., Olsen, J., Reinig, F., Sakamoto, M., Sookdeo, A., Talamo, S., 2020b. The IntCal20 Northern Hemisphere radiocarbon calibration curve (0–55 cal kBP). Radiocarbon 62 (4), 725–757. https://doi.org/10.1017/RDC.2020.41.

Sagawa, T., Nagahashi, Y., Satoguchi, Y., Holbourn, A., Itaki, T., Gallagher, S.J., Saavedra-Pellitero, M., Ikehara, K., Irino, T., Tada, R., 2018. Integrated tephrostratigraphy and stable isotope stratigraphy in the Japan Sea and East China Sea using IODP Sites U1426, U1427, and U1429, Expedition 346 Asian Monsoon. Prog. Earth Planet. Sci. 5 (1), 1–24. https://doi.org/10.1186/S40645-018-0168-7.

Schindlbeck, J.C., Kutterolf, S., Straub, S.M., Andrews, G.D.M., Wang, K.-L., Mleneck-Vautravers, M.J., 2018. One Million Years tephra record at IODP Sites U1436 and U1437: insights into explosive volcanism from the Japan and Izu arcs. Island Arc 27 (3), e12244.

Schlolaut, G., Marshall, M.H., Brauer, A., Nakagawa, T., Lamb, H.F., Staff, R.A, Bronk Ramsey, C., Bryant, C.L., Brock, F., Kossler, A., Tarasov, P.E., Yokoyama, Y., Tada, R., Haraguchi, T., 2012. An automated method for varve interpolation and its application to the late Glacial chronology from Lake Suigetsu, Japan. Quat. Geochronol. 13, 52–69. https://doi.org/10.1016/j.quageo.2012.07.005.

Schlolaut, G., Staff, R.A, Brauer, A., Lamb, H.F., Marshall, M.H., Bronk Ramsey, C., Nakagawa, T., 2018. An extended and revised Lake Suigetsu varve chronology from ~50 to ~10 ka BP based on detailed sediment micro-facies analyses. Quat. Sci. Rev. 200. https://doi.org/10.1016/j.quascirev.2018.09.021, 351–36.

Smith, V.C., Staff, R.A, Blockley, S.P.E., Bronk Ramsey, C., Nakagawa, T., Mark, D.F., Takemura, K., Danhara, T., 2013. Identification and correlation of visible tephras in the Lake Suigetsu SG06 sedimentary archive, Japan: chronostratigraphic markers for synchronising of east Asian/West Pacific palaeoclimatic records across the last 150 ka. Quat. Sci. Rev. https://doi.org/10.1016/j.quascirev.2013.01.026.

Sulpizio, R., Zanchetta, G., Caron, B., Dellino, P., Mele, D., Giaccio, B., Insinga, D., Paterne, M., Siani, G., Costa, A., Macedonio, G., Santacroce, R., 2014. Volcanic ash hazard in the Central Mediterranean assessed from geological data. Bull. Volcanol. 76, 866. https://doi.org/10.1007/s00445-014-0866-y.

Staff, R.A, Ramsey, C.B., Bryant, C.L., Brock, F., Payne, R.L., Schlolaut, G., Marshall, M. H., Brauer, A., Lamb, H.F., Tarasov, P., Yokoyama, Y., Haraguchi, T., Gotanda, K., Yonenobu, H., Nakagawa, T., 2011. New ^{14}C determinations from Lake Suigetsu, Japan: 12,000 to 0 Cal BP. Radiocarbon 53 (3), 511–528. https://doi.org/10.1017/S0033822200034627.

Sulpizio, R., Costa, A., Massaro, S., Selva, J., Billotta, E., 2024. Assessing volumes of tephra fallout deposits: a simplified method for data scarcity cases. Bull. Volcanol. 86 (7), 62.

Sun, C., Plunkett, G., Liu, J., Zhao, H., Sigl, M., McConnell, J.R., Pilcher, J.R., Vinther, B., Steffensen, J.P., Hall, V., 2014. Ash from Changbaishan Millennium eruption recorded in Greenland ice: implications for determining the eruption's timing and impact. Geophys. Res. Lett. 41 (2), 694–701. https://doi.org/10.1002/2013GL058642.

Takada, H., 1989. Preliminary report on tephra from Aso central cones. J. Kumamoto Geosci. Assoc. 90, 8–11 (in Japanese).

Takarada, S., Hoshizumi, H., 2020. Distribution and eruptive volume of Aso-4 pyroclastic density current and tephra fall deposits, Japan: A M8 super-eruption. Front. Earth Sci. 8, 170.

Tomlinson, E.L., Thordarson, T., Muller, W., Thirlwall, M., Menzies, M.A., 2010. Microanalysis of tephras by LA-ICP-MS- strategies, advantages and limitations assessed using the Thorsmork ignimbrite (Southern Iceland). Chem. Geol. 279, 73–89. https://doi.org/10.1016/j.chemgeo.2010.09.013.

Tsuji, T., Ikeda, M., Furusawa, A., Nakamura, C., Ichikawa, K., Yanagida, M., Nishizaka, N., Ohnishi, K., Ohno, Y., 2018. High resolution record of Quaternary explosive volcanism recorded in fluvio-lacustrine sediments of the Uwa basin, Southwest Japan. Quat. Int. 471, 278–297. https://doi.org/10.1016/j.quaint.2017.10.016.

Vineberg, S.O., Isaia, R., Albert, P.G., Brown, R.J., Smith, V.C., 2023. Insights into the explosive eruption history of the Campanian volcanoes prior to the Campanian

Ignimbrite eruption. J. Volcanol. Geotherm. Res. 443. https://doi.org/10.1016/j.jvolgeores.2023.107915.
Vineberg, S.O., Albert, P.G., McLean, D., Suzuki, T., Staff, R.A, Yamada, K., Kitaba, I., Kitagawa, J., Manning, C.J., Buckland, H.M., Jones, G., 2024. A detailed record of large explosive eruptions from Japan between~ 120 and 50 ka preserved at Lake Suigetsu. Quat. Sci. Rev. 346, 109021.
Watanabe, K., Ono, K., Hiratsuka, S., 1982. Pumice eruption at Kusasenrigahama volcano. Bull. Volc. Soc. Jpn. 27, 337–339.
Watanabe, K., Fujimoto, M., 1992. Subsurface geological map of Asosan and Taketa. Kumamoto Prefectural Government, pp. 15–28 (in Japanese).
Wulf, S., Kraml, M., Brauer, A., Keller, J., Negendank, J.F., 2004. Tephrochronology of the 100 ka lacustrine sediment record of Lago Grande di Monticchio (southern Italy). Quat. Int. 122 (1), 7–30.
Wulf, S., Keller, J., Paterne, M., Mingram, J., Lauterbach, S., Opitz, S., Sottili, G., Giaccio, B., Albert, P.G., Satow, C., Tomlinson, E.L., Viccaro, M., Brauer, A., 2012. The 100-133 ka record of Italian explosive volcanism and revised tephrochronology of Lago Grande di Monticchio. Quat. Sci. Rev. 58, 104–123.
Wutke, K., Wulf, S., Tomlinson, E.L., Hardiman, M., Dulski, P., Luterbacher, J., Brauer, A., 2015. Geochemical properties and environmental impacts of seven Campanian tephra layers deposited between 40 and 38 ka BP in the varved lake sediments of Lago Grande di Monticchio, southern Italy. Quat. Sci. Rev. 118, 67–83.